RADAR STUDIES OF ARCTIC ICE

by

J. W. Rouse, Jr.

J. A. Schell

Get DRA

Invited Presentation for the

Defense Research Establishment of Ottawa
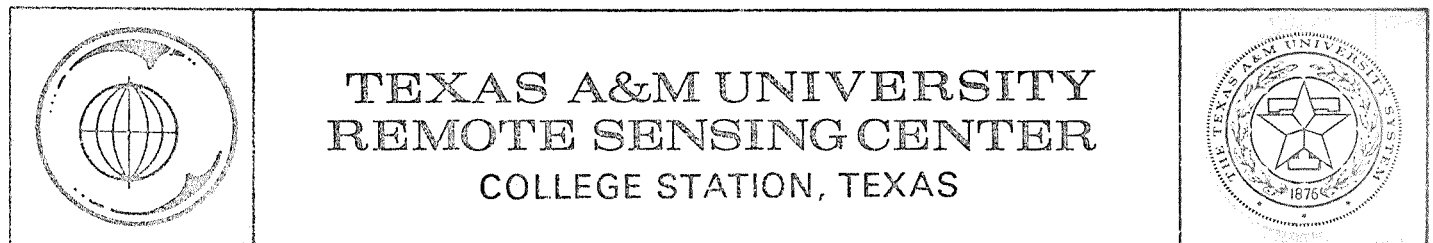Ottawa, Ontario, Canada

October 1970

TEXAS A&M UNIVERSITY
REMOTE SENSING CENTER
COLLEGE STATION, TEXAS

RADAR STUDIES OF ARCTIC ICE

by

.J. W. Rouse, Jr. and J. A. Schell
Texas A&M University

ABSTRACT - Analysis of 2.25 cm wavelength radar measurements of Arctic ice recorded by NASA has shown that identification of several different ice types is possible. The identification accomplished in this analysis depends almost entirely upon radar return effects due to surface topography. In laboratory tests using simulated radar data which contained effects due to topography only, it was found that near real-time identificaiton of some ice types could be accomplished using a relatively simple electronic network. This paper summarizes the results of the analysis and describes the system simulation.

A qualitative model for sea ice backscatter is proposed which emphasises surface topography and near-surface volumetric scattering as the dominant factors effecting the radar return. The model, which incorporates recent experimental results of depolarization dependence, suggests a new approach to interpretation of radar backscatter from sea ice.

RADAR STUDIES OF ARCTIC ICE

by

J. W. Rouse, Jr. and J. A. Schell

INTRODUCTION

The measurements of radar backscatter obtained by a National Aeronautics and Space Administration aircraft in 1967 constitute one of the few known sets of data available of a form and quality suitable for evaluation of the capability of airborne radar to identify sea ice types. An analysis of these data by Rouse (1969) clearly established the potential of ice type identification by radar. Subsequent studies at Texas A&M University confirmed these results and showed that data of higher quality and greater variety, e.g. multi-frequency multi-polarization, etc. was required before the full potential of the sensor could be properly accessed.

The radar analysis, which is reviewed in this paper, utilized properties of the backscatter predominantly determined by surface topography. The quality of the data would not support conclusions based upon surface composition changes, however such changes were evident in the data as expected in view of the differences

in physical characteristics among various types of sea ice. Incorporation of the dielectric properties of sea ice into the data analysis procedure is shown to be the necessary next phase of the study.

The analysis effort utilized a variety of statistical techniques in establishing the correlation between the radar measurements and the sea ice distributions. Some of these methods were of a form adaptable to simple electronic analog computer networks. This laboratory network provided a means to process the analog radar output signal for real-time determination of certain ice types responsible for the radar return.

Recent experimental observations of the backscatter characteristics of coherent light conducted by Leader (1970) suggest a new scattering model adaptable to sea ice studies. The most significant property of this model is the high degree of dependence of the depolarized backscatter upon dielectric properties of a scattering volume near the surface. The salt-water ice attenuation studies by Hoekstra (1969) have already established that the "layer" model commonly used for analysis of freshwater ice backscatter is inappropriate for sea ice.

A volumetric scatter model which incorporates rough surface scatter and inhomogeneous volume scatter is suggested.

ARCTIC ICE RADAR RETURN

In May, 1967, the NASA 927 P3A (Electra) remote sensor aircraft flew repeated missions near Pt. Barrow, Alaska, to record data from Arctic ice. The primary flights were over selected lines at Pt. Barrow, which were established and documented by CRREL personnel (headed by J. McLerran) and Arctic Institute personnel, and over two lines located approximately 150 nm north-northeast of Pt. Barrow. One of these lines was documented by a Navy Oceanographic Office team (headed by R. D. Ketchum) camped at the site. In addition, several lines were selected at random during the flights. The data collected included black-and-white photography, color IR photography, X-band radiometer images, IR images, and 2.25-cm radar scatterometer measurements. Due to the extreme cloud cover experienced daily during the mission, much of the photography and imagery is degraded; however, the

radar data are reasonably good, and constitute the most highly controlled radar measurements of Arctic ice known to exist.

Radar scatterometers measure variation of the scattering coefficient of surfaces with incidence angle. Scatterometer measurements permit a more detailed observation of radar scattering behavior than radar images, although the resolution and area coverage are poorer. The NASA scatterometer used in this measurement program was a 2.25 cm wavelength Ryan Redop system. This radar transmits a vertical-polarization CW signal in a "fan-beam" antenna pattern. The illuminated area is 120° (±60°) fore-aft along the aircraft flight line and 3° (±1.5°) port-starboard.

The radar return was recorded on magnetic tape and subsequently processed through a set of Doppler filters. Each filter represented a discrete incidence angle within the 0°-to-60° (fore and aft) beam, e.g., 2.5°, 7.2°, 15°, 25°, etc. The filter frequencies correspond to the incidence angle according to the relation

$$f_d = \frac{2v\sin\theta}{\lambda} \tag{1}$$

where: f_d = Doppler frequency shift

v = relative velocity of radar

θ = incidence angle

λ = wavelength

Since the entire 120° × 3° region is continuously illuminated, the entire scattering coefficient versus incidence angle curve fore and aft is recorded during a single overflight. By suitable processing of the return signal, a scattering coefficient versus incidence angle plot was obtained which shows the scattering coefficient variation for particular terrain "cells" along the flight line. This is done by delaying in time the signal outputs of each Doppler filter. By appropriate choice of each time delay, we obtained the effect of viewing one spot on the terrain from several angles simultaneously. The data shown in this paper are the scattering coefficients for adjacent "cells" on the ice about 30 meters square. Since the radar returns are recorded in quadrature, the fore-beam and aft-beam data are separated. The results shown here are fore-beam measurements only.

The radar scatterometry data analysis concentrated on three flight lines designated line 92, line 94, and line 91.

Line 92

    In Fig. 1 is shown a segment of line 92
located approximately 150 nm north-northeast of Pt.
Barrow, Alaska. This segment consists of a large
multiyear ice floe (to the left of A), rough first-
year ice (region F), smooth first-year ice (regions
B and D), and two small multiyear pieces about 100
meters long (located at C and E). This line was
documented by a NAVOCEANO team camped on the old ice
floe. Their report shows the old ice floe to be sev-
eral years in age. It is well weathered, and the
hummocks are well rounded. The peaks of the ridges
are bare ice, and the depressed areas contain snow
varying in depth between 20 and 60 cm. The first-
year ice has an average thickness of 1.35 meters and
is reasonably uniform. It is covered by numerous
scattered blocks of ice; however, the snow cover is
only 1-2 cm. The hummocking is mild, and most ridges
are less than 1 meter high, except in region F where
the hummocking is more dense. The pressure ridge
bordering the old ice floe is approximately 2 meters
high.

Line 94

     In Fig. 2 is shown a segment of line 94 which is located parallel to line 92 and displaced approximately 5 miles. The ice types and conditions present in the line are similar to those described in line 92. Referring to the photo mosaic, the prominent boundaries are at B, which denotes a boundary between ridged and smooth first-year ice; D, which denotes a boundary between smooth first-year ice and multiyear ice at an open water crack; I, which denotes a boundary between multiyear ice and smooth first-year ice; and K, which denotes a high pressure ridge dividing two sections of smooth first-year ice.

     The radar scatterometer profile is labeled to show the close correlation of the radar data with the various ice areas. The high return shown at K is from a pressure ridge running through the first-year ice. From the profile shown in Fig. 2 at 25° incidence angle there is little differentiation between the area of pressure-ridged first-year ice labeled K and the old region, D through I. However, this region (D through I) was clearly delineated,

utilizing data from other angles, as is evident upon examining the σ^0 versus θ plots for the different regions. As an example, the scattering coefficient from 7.2° and 51.7° incidence angles are plotted against each other in Fig. 3. The data indicated on the graph by circles are from the old-ice section (D through I). The triangles indicate data to the right of the boundary at D, and the solid dots indicate data to the left of the boundary at I. In this graphical method of data comparison the returns from the old ice form a set labeled 1 in Fig. 3. The points in the region labeled 2 are from two large pressure-ridge regions, one at the area labeled A of Fig. 2 and the other at K. The region labeled 3 of Fig. 3 represents data from the very smooth first-year ice to the left of K in Fig. 2. (Most of the region is not shown on the air photo mosaic.) The data in category 4 are from a combination of smooth and mildly ridged first-year ice.

Line 91

The categories illustrated by Fig. 3 show
a clear differentiation of multiyear ice and areas of
major pressure ridging; however, differentiation be-
tween smooth first-year ice and mildly ridged first-
year ice is not sufficiently distinct to make positive
identification between types. Therefore, data from
a region of exclusively first-year ice were examined.
This segment (line 91) is shown in Fig. 4. From the
scatterometry data profile accompanying the photo
mosaic it is evident that the ice-water boundaries
at A and F are clearly shown. Likewise, the cracks
at area B are evident by "spiking." However, the
transition between smooth first-year ice in areas C
through F is not as distinct. A boundary is noted
at C between smooth first-year ice and the crumbling
block structure at a major pressure ridge. Similarly,
the transition through the relatively large, smooth
ice section shown at D is evident in the scatterometry
data. Clearly, however, the sharp contrast noted in
Fig. 2 between old ice and first-year ice is not evi-
dent in Fig. 4, which consists only of first-year ice
in two states, smooth and ridged.

Point-by-point comparison of the scattering coefficient curves for three regions in each line shown in Figs. 1, 2, and 4 indicates that the measurements of the two regions of old ice in line 92 are in good agreement. The distinction between the return from the old ice in line 94 and the region K return is an approximate 3-dB difference in curves to 25° with an increasing difference beyond 25°, and the two regions of first-year ice in line 91 are very similar except for the more rapid flattening of the curve for ridged ice.

In Fig. 5 the scattering coefficient curves for the first-year ice regions in lines 92 and 94 are compared with the ridged first-year ice region in line 91. The agreement, especially in shape, is good. The smooth first-year ice region in line 91 exhibited too great a slope near the vertical for good agreement with the results of lines 92 and 94. The first-year ice in line 91 (region B) is very smooth relative to the block-strewn first-year ice of the more northern ice in lines 92 and 94. In Fig. 6 the multiyear ice measurements of line 92 are compared with the multiyear ice of line 94. The agreement is good to 35°.

Thereafter the line 92 curves are much higher for both old-ice regions.

Visual comparison of the results gives some insight as to the behavior of the return. Detailing the comparisons as in Fig. 3 verifies the "signature" characteristics, and extending this approach to multiple angles, i.e., three- and four-dimensional comparisons, further emphasizes ice type discrimination. However, such approaches are quantitative, and a more specific means of categorizing is desired.

CATEGORIZATION TECHNIQUES

It is evident from the quantitative analysis presented that the data have distinctive characteristics associated with the ice type responsible for the radar return. There are numerous statistical techniques which can be employed to categorize these features, of which the following represent useful examples. These techniques include a single variable method based on a backscatter theory popularly known as the Kirchhoff method, various empirical polynomials, general cluster analysis, and pattern classification techniques using minimum distance and Bayes maximum likelihood criteria.

Kirchhoff Method

One analysis technique used was based on the Kirchhoff method previously used by Rouse (1969) and subsequently adapted for the computer by Eppes (1969). The technique consists of fitting a functional relationship to the data.

The computer analysis technique used by Eppes to fit the functional relationship was based on the method of least squares, an application of prediction analysis as described by Wolberg (1967). A set of parameters is iteratively adjusted so that the sum of the mean-squared error is a minimum.

The functional relationship used is obtained from an equation developed by Hagfors (1964) using the Kirchhoff method of describing scattering energy from surfaces whose characteristics are described by an exponential autocorrelation function. The relation is:

$$\sigma^0 = k \log (\cos^4\theta + S \sin^2\theta) \qquad (2)$$

where: σ^0 = average scattering coefficient

θ = incidence angle from nadir

S = surface roughness factor

In using this technique it is assumed that the surface
roughness factor S will have values characteristic of
the surface types responsible for the radar returned.

Since the Kirchhoff equation describes nor-
malized energy returned from an illuminated surface in
db, values of the scattering coefficient are expected
to be negative. This however is not always the case
for values determined for Mission 47. Average values
of σ^0 vary from line to line over similar ice types as
mentioned before and in many cases values for σ^0 were
positive. The first values for the surface roughness
factor were obtained by normalizing each data cell to
its largest value of σ^0 and then applying the fitting
program to find the best fit. This approach would
generally categorize the shape of the curve and avoid
the problem of dc shift. These values of the surface
roughness factor were determined for the first angles
of each data cell (i.e. 2.5°, 3.0°, 7.0°, 15.0°, and
25.0°) and the average values of the surface roughness
factor for the training sets are tabulated as SRF in
Table 2 for the ice types shown in Table 1.

The large values of surface roughness factor
indicate a generally smoother surface. Thus, for example,
the surface roughness factor obtained for water/new ice

in line 91 is significantly larger than for the various
types of first year ice.

In the lines where first year and multi-year
ice are present, it is apparent from the surface rough-
ness factor that the multi-year ice is rougher than
first year ice. This might indicate a more volumetric
roughness as previously considered. In comparison be-
tween first year types, types II and VI appear smoother
than the other types as expected; however, type II ice
has a smaller surface roughness factor than type II.
Type I ice is broken type II ice, and due to large
pieces holding together, its surface roughness factor
on an average is larger than would be apparent from
the photography. The training region for type III
appears to be slightly ridged, and the snow appears
to have banked in that region. Thus, it is possible
that more volumetric scattering is apparent from the
type III ice.

In order to utilize the effect of the average
shift in the data, the Kirchhoff equation described
previously was modified by the addition of a constant.
Thus the modified Kirchhoff equation became

$$\sigma^0 = k \log (\cos^4\theta + S \sin^2\theta) + b \qquad (3)$$

where: b = a constant

This equation was then fit, using the Eppes analysis program, varying the two parameters S, the surface roughness factor, and b, the constant shift. In order to get as broad an averaging as possible, the angles selected were 2.5°, 7.0°, 15.0°, 25.0°, 35.0°. These results are averaged for the training sets and presented in Table 2 as SRF_2 and CON. The clustering of these parameters is shown in Figures 7-9.

Polynomial Fit

It was felt that an equation more suitable for machine implementation might be empirically found to fit the data. Since a linear system is most easily built, the search for functions to fit the data was limited to linear polynomials. These polynomials were selected so that their coefficients might describe either the shift in the data due to changing dielectric constant or the variations due to surface roughness. The polynomials were also selected to fit the shape of the average data curves.

The polynomials selected for analysis were tried on data (angles 7.0°, 15.0°, 25.0°, 35.0°, and

51.0°) from line 94 to test their applicability and closeness of fit. They are listed in Table 3 with their average least squared error for the points in line 94.

The coefficients of each polymonial were presented on a cluster chart. The most significant clustering occurred for Equation II between a and b coefficients. This polynomial was subsequently selected for analysis of each line, and the clustering is shown in Figures 10-12. Average values for the training sets are shown in Table 4.

Pattern Classification

Pattern classification techniques are being used in many fields of study to identify objects and their parameters from multi-dimensional measurements. The measurements of the parameter which uniquely characterize an object constitute a signature by which the object can be identified. Similar objects can be distinguished by the characteristics in which they differ.

The intellectual tasks of learning and comparing must be mechanized so that a machine has the

ability to learn signatures. It must also be able to compare and sort new data according to the identity of the object presented. In order to accomplish these tasks, a mathematical model or machine is developed so that each new data set (or pattern) is compared with previous knowledge and the machine responds with the correct classification.

One way of accomplishing this identification is the development of discriminant functions from measurements of known objects. Two essential properties of these functions are that they must be real and single valued and that the value of the discriminant function corresponding to the correct class classification for a particular pattern must have the largest value compared to other values of discriminant functions for that pattern. Thus a data point is classified as belonging to the category whose discriminant function is largest for that data point.

Since linear functions are generally simple to implement, several commonly used discriminant functions were selected to analyze the scatterometer data. The first discriminant function selected was based on the maximum-likelihood or Bayes decision cri-

teria. This approach assigns the pattern to the category for which the probability of the pattern occurring for that category is greatest. This method assumes that the probability density function is known. Discriminant functions are expressed in terms of these probability functions and their parameters.

The most commonly used classifier of this type is developed from multivariate Gaussian distribution where each category is assumed equally probable. The means and variances of these distributions are assumed to be the means and variances of the training sets (data for which the classification is assumed or known). In this case the discriminant function becomes:

$$g_i(X) = \log p_i - \frac{1}{2} \log |\Sigma| - \frac{1}{2} [X-M_i]^T \Sigma^{-1} [X-M_i] \qquad (4)$$

where: X = is the n-dimensional pattern

$g_i(X)$ = is the discriminant function of the ith category

p_i = is the probability of the occurrence of the ith category

M_i = mean pattern of the ith category training set

and Σ = is the covariance matrix of the training set

The second discriminant function selected was based on the minimum distance criteria. In this case the mean values of the pattern vectors are computed for each category. A pattern is then assigned to the category to which it is closest (in some sense) to the mean. In this case the normal Euclidian concept of distance was used and the discriminant function subsequently becomes

$$g_i(X) = X - P_i - \frac{1}{2} P_i \cdot P_i \qquad (5)$$

where: P_i is the mean value of the training set and $g_i(X)$ and X are the discriminant function and pattern as before.

These two classification algorithms were tried on the data with the sets which were classified from the ground photography taken as training sets. The resultant classification of the data was compared with the ground photography mosaics. The minimum distance technique worked well in classifying all of the lines. The Bayes criteria however, failed in the classification because of the strong correlation between the data at each angle. The use of this particular technique was abandoned in favor of the minimum distance criteria in further iden-

tification.. A disadvantage of the minimum distance criteria is the weighting of the discriminant function by the larger elements of the pattern.

It was not possible in general to obtain a one-to-one correspondence between the data cells and a point on the ground. Therefore, major homogeneous areas were selected from the flight line and data points from well within these boundaries were selected for comparison. The results of classification in these regions is shown in Table 5 where the total number of points, those correctly classified, those points classified in a related category (a first-year type as another first-year type) and the number of grossly incorrect classification are listed.

Clustering Techniques

Several analyses were conducted in an attempt to determine computed parameters which might be used to distinguish ice types. These analyses consisted essentially of selecting parameters and presenting them on a cluster plot to observe the degree of similarity in a class and the separation between classes.

Among the parameters investigated were surface roughness factor, slope of a best-fit line through the data, its zero degree intercept and the average value of the data. The best grouping and inter-classification separation occurred for the slope-average value plots which are presented in Figures 13-15. Average values for the training sets are shown in Table 6.

Several normalization techniques were applied between lines in an attempt to reduce the effect of the data discrepancies. The most successful of the techniques attempted was the normalization of each line about a major ice category common to each. In this case first-year ice was used, and it was noted that the major classes separated sufficiently to allow gross classification by merely observing the data. In Figure 16 the cluster plot of the normalized slope and average value are shown for the points from the three lines. In this normalization the average values of the slope and average for first-year ice were determined and these were subtracted from all the data points. The three major categories cluster well. Transition points are those which fall outside of the major cluster. Due

to the shortage of data from other lines and the emphasis on distinguishing variations within major categories, the normalization concepts were not developed further.

Each of the analysis techniques applied was successful, to varying degrees, in classifying major groupings of ice where the classification was limited to the lines in which the training was done. It appeared from these analyses and from attempts at data normalization that the dielectric shift as well as the roughness characteristic were necessary in the classification of data.

One specific technique can not be singled out as being far better than the others, because of the limited nature of the data and the limited number of data points per training set (particularly in types of first-year ice) do not present a sufficiently broad base upon which a decision could be founded. However, the slope-average, modified Kirchhoff, and minimum distance pattern classification techniques seem to offer the best discrimination between subclasses in the first-year ice.

SCATTEROMETER SIGNAL PROCESSING

The radar scatterometer transmit a fan beam signal which is scattered by the terrain providing a return signal to the radar which varies both in amplitude and frequency. This doppler frequency shift is dependent upon the velocity of the aircraft, its altitude and the angle at which the terrain cell is viewed. The amplitude of the return depends upon the angle of illumination and the complex interaction of the terrain and the radar signal. Thus the scatter from the terrain for a specific angle occurs in the received signal at a unique frequency and decoding of scatterometer data for an angle requires the separation of its particular frequency from the total return.

In present scatterometer systems the return signal is processed so that it might be recorded on magnetic tape. This is accomplished by a translation of the return signal from the microwave frequencies to the audio doppler shift frequencies which can be conveniently recorded on magnetic tape. As a consequence of this processing, the signals from the aft data cells are folded onto those from the fore cells. To enable

the separation of the fore and aft data the return
signal is quadrature shifted and then frequency trans-
lated as above to provide a second output signal, thus
the output from the scatterometer system consists of
two channels of data at audio frequencies which are
subsequently recorded on magnetic tape.

The scatter at a particular angle can be ob-
tained by extracting the information from these channels
by filtering at the corresponding doppler frequency.
This filtering can be accomplished by either digital or
analog methods. By detecting and adding these doppler
signals from the two channels, the fore data at the
specified angle can be extracted.

The set of data used to characterize a ground
data cell is the scatter from that cell at several an-
gles. To obtain this information for a data cell the
signals from the desired angles are time shifted so
that the returns from the cell align. These signals
are converted to values of the scattering coefficient
by application of the radar equation. This set of scat-
tering coefficients is essentially the data used for
terrain characterization by airborne scatterometer meas-
urements.

CLASSIFIER SIMULATION

A simple simulation of radar scatterometer data was made using audio frequencies to test the feasibility of a system scheme for the near real-time identification of ice type. Scattering coefficients, calculated from Mission 47 were encoded by amplitude modulation of sinusoidal signals at simulated doppler shift frequencies. These signals, representing the return at several angels, were summed to provide the signal used to represent the scatterometer return signal. This was recorded on analog magnetic tape.

In subsequent processing, this signal was filtered at the simulated doppler frequencies and these outputs were magnitude detected to present the backscatter return to the classification system. The phases of processing which include the shifting of the data, the separation of fore and aft data and the subsequent calculation of scattering coefficient were not attempted at this time. The primary purpose of the experiment was to determine the relative worth of an analog classification scheme.

ANALOG IMPLEMENTATION

The analog circuitry was used here to perform three basic functions. It provided the active portion of the bandpass filters, it provided preliminary signal processing resulting in classification parameters, and it provided for implementation of the classification algorithm. An analog approach was taken primarly because of the simplicity of the overall system scheme and the versatility of analog computation for the solution of linear equations. Other valid reasons for an analog implementation are the following:

    a) nearly instantaneous computation

    b) ease of parameter adjustment

    c) compatability with analog outputs

    d) ease in implementation of integration.

Three basic analog circuits were used in this experiment and are shown in Figure 17. The first is the analog adder. As is depicted several signals, in this case x_1, x_2, and x_3 are presented to the adder network with variable coefficients A_1, A_2, A_3 and the output is the linear polynomial shown. The second circuit used is a band-pass filter which allows only a

narrow band of frequencies near its center frequency f_0 to pass unattenuated. The third circuit, a comparator determines the sign of its input and provides an output voltage at V_1 or V_2 accordingly. It is combinations of these three basic circuits which make up the described system.

The classification portion of the identification system was implemented by the programming of linear discrimination functions. This general class of discriminant functions allows implementation over a broad range of decision criteria. Among the permissible criteria are minimum distance to the mean, maximum likelihood among certain distributions, and others for which the discriminant function reduces to a linear equation.

This form of classification analysis calls for division of the parameter space by hyperplanes into the various sections containing the accumulation of points belonging to the desired classes. This is accomplished in the case of two classes by programming a linear function which has the value zero along the boundary between the two classes. Thus if the function evaluated at a point has a positive value, that point

may be considered as belonging to one class, and to the other if the value of the function is negative. This is represented for two classes in Figure 18. For a larger number of classification parameters or classes this technique can be expanded by the addition of the appropriate logic circuitry.

In this simulation the minimum distance to the mean was selected as the decision criteria and the identification was restricted to two classes and three dimensions. All data points producing a value of the discriminant function greater than zero are classified as belonging to class II and those producing values of less than zero are classified as belonging to class I.

Values of the scattering coefficients were taken from line 94 and the two classes considered were multi-year ice and first-year ice. Two procedures were used in obtaining values for the classification parameters. In the first the actual values of the scattering coefficients at several angles (7.2°, 15.0°, 25°) were used and the identification system essentially compared the input scattering coefficient values with the average scattering coefficients of the training sets.

This is the implementation of the procedure described in the proceeding section on Pattern Classification.

In the second procedure, the input scattering coefficients were fit by a linear polynomial (Table 3, II). If the data angles and the polynomial are fixed, and the number of measurements is greater than the number of terms of the polynomial, the determination of the coefficients of the polynomial (which is the best least square fit to the data) reduces to the calculation of a set of linear equations readily implemented on the analog computer. These coefficients were then used as classification parameters.

In Figure 19 is shown the circuitry for the classification procedure. The magnetic tape unit on which the simulated signal was recorded appears on the left. The signal from the recorder is passed through filters and is detected to provide values for the scattering coefficient at three angles. In the parameter calculation section, three calculations are made to determine the coefficients of the best fit of linear polynomial. These coefficients are then presented as classification parameters to the circuitry providing the discriminant implementation. The calculated value of

the discriminant function is then presented to the comparator which provides the driving voltage for the classification indicators.

A number of data points were introduced to the system in this manner to determine what degradations could be expected in an analog implementation of a classifier. It was determined that the analog system classified data as well as the corresponding implementation on a general purpose digital computer and that the major problem in this system is the determination of a suitable identification algorithm for classification of ice types.

This simulation has shown that an analog identification system for certain algorithms can be built rather simply, at an expected lower expense than a corresponding digital system. It has also shown that the degradation of identification in an analog system is not appreciably different than a digital system and depends primarily on the identification algorithim used.

QUANTITATIVE SEA ICE MODEL

A popular model used to describe electromagnetic scatter from sea ice has been the "layer" model applicable to fresh water ice, with the addition of a diffuse interface between the water and the underside of the ice. For this model, the boundary values at the upper ice surface satisfy the descriptive equation, i.e. the ice media is considered infinitely thick. The attenuation measurements by Hoekstra suggest that the ice-water boundary is seldom excited by incident radar signals, except for very thin ice, and that the near-surface volume controls the scattering characteristics. Following accepted practices of estimating scattering behavior at an interface, the fact that the attenuation of sea ice is higher than previously imagined would not alter the approach, but would merely change the reflection coefficient, hence altering the magnitude of the calculated radar cross section.

Experimental data have been reasonably well fit using theory based upon such a model and elaborate rationalization has been developed to justify its case. However, recent experimental observations by Leader (1970) suggest a somewhat different model which

could have considerably importance to interpretation
of sea ice radar return.

Electromagnetic scatter theory for rough
surfaces has advanced rapidly in recent years. Several
different approaches had been advanced including the
popular Kirchhoff method (Beckmann and Spizichino 1964)
and the small perturbation technique (Rice 1951). The
Kirchhoff method generally fails to correctly estimate
backscatter from angles removed from the vertical.
The small perturbation method more accurately predicts
the backscatter from the mid-angles, but fails near the
nadir and the assumptions about the nature of the rough
surface are difficult to substantiate for natural ter-
rain. One of the most unexplainable characteristics of
the Kirchhoff method is that it cannot account for any
significant depolarized component in the backscatter
direction. The small perturbation does predict a de-
polarization component caused by a surface scattering
phenomena. The merger of these two techniques using a
composite surface concept (Semyonov, 1966; Fung and
Chan, 1969; Wright, 1968) have proven very successful
for explaining several previously unmanageable char-
acteristics of radar measurements of natural surfaces.

In the context of radar studies of Arctic ice, the development of these general scattering theories should improve the ability to relate back-scatter measurements to surface parameters. Unfortunately, only surface parameters have appreciable effect on the theoretically predicted behavior of the radar return. Ideally the very distinctive character of the near-surface volume of ice would be influential in the scattering behavior. The nonhomogeneous, anisotropic upper volume of sea ice is highly type or age dependent and, if recorded in the radar backscatter, it should substantially improve the ice type identification capability of the sensor.

The coherent optics experiments by Leader provide strong evidence that the general scattering theories discussed above are inadequate for predicting sea ice backscatter, especially for the depolarized component. Leader showed that a theory based on the Kirchhoff-Huygens principle can satisfactorily estimate scatter from a wide range of rough surfaces. More importantly, his work established that the Kirchhoff method correctly predicted the lack of any significant depolarization of the scatter in the plane of incidence. This

phase of the experiment employed an optically "black"
surface for which there were no contributions from the
volume, i.e. the scatter was completely surface depen-
dent. In a subsequent test using the same surface
roughness on a material for which a volume scatter
component did exist, a depolarization component did
exist. In addition, he showed that by subtracting the
depolarized scatter energy from the polarized scatter
energy, the results matched those previously recorded
for the "black" material. It was concluded that the
depolarized component was the result of a near-surface
volumetric scattering phenomenon.

This feature is not incorporated into any of
the general rough surface scatter theories and consid-
erably more experimentation will be required before an
appropriate description is possible. However, the rec-
ognition of the potential existance of a strongly ma-
terial related component in the radar return offers a
new approach to interpretation of radar backscatter
measurements of sea ice.

CONCLUSION

Using the angular dependence characteristics, a predominately topography related parameter, of 2.25 cm wavelength backscatter from Arctic ice, identification of certain sea ice by type is possible. Several data analysis techniques developed to establish the backscatter correspondence to sea ice type are amenable to simple electronic hardware implementation which offer the potential for near real-time identification of specific ice types. In addition, a new model, based on recent laboratory experiments, indicates the potential for improved radar identification of Arctic ice by incorporation of the depolarized component.

REFERENCES

P. Beckmann and A. Spizzichino, The Scattering of Electro-
    magnetic Waves from Rough Surfaces, New York;
    MacMillan, 1963.

T.A. Eppes, "Discussion of a Least Squared Technique and
    Development of a Curve Fitting Subroutine," Technical
    Report RSC-04, Remote Sensing Center, Texas A&M Univ-
    ersity, September 1969.

A.K. Fung and H.L. Chan, "Backscatter of Waves by Composite
    Rough Surfaces," IEEE Trans. Antennas and Propagation,
    vol. AP-17, no. 5, pp 590-597, September 1969.

T. Hagfors, "Backscattering from an Undulating Surface with
    Applications to Radar Returns from the Moon," J.
    Geophys.Research, vol. 69, no 18, pp 3779-3784, 1964.

J.C. Leader, "Bidirectional Scattering of Electromagnetic
    Waves from Rough Surfaces," presented at the Spring
    USNC/URSI Meeting, Washington D.C., April 16, 1970.

S.O. Rice, "Reflection of Electromagnetic Waves from Slightly
    Rough Surfaces," Comm. Pure and Appl. Math, vol. 4,
    no 4, 1951.

J.W. Rouse, Jr., "Arctic Ice Type Identification by Radar,"
    Proc. IEEE, vol. 57, no 4, pp 605-611, April 1969.

B.I. Semyonov, "An Approximate Calculation of Scattering of
    Electromagnetic Waves from Rough Surfaces," Radioteckh.
    Elektron., vol. 11, pp 1351-1361, August 1966.

J.R. Wolberg, Prediction Analysis, Princeton: Van Nostrand,
    1967.

J.W. Wright, "A New Model for Sea Clutter," IEEE Trans.
    Antennas and Propagation, vol. AP-16, no 2, pp 217-223,
    March 1968.

TABLE 1

ICE TYPE DEFINITION

Type	Surface
I	Broken First-Year Ice
II	Smooth First-Year Ice
IV	Snow Covered First-Year Ice
IV	Water And/Or New Ice
V	Multi-Year Ice
VI	Weathered, Snow-Covered First-Year Ice

TABLE 2

KIRCHHOFF EQUATION RESULTS

Type	Line	SRF	SRF_2	CON
I	91	11.9	7.43	-2.80
II	91	21.3	14.63	0.02
II	94	62.8	47.67	0.44
III	91	6.1	5.72	-3.54
IV	91	76.6	63.14	7.46
V	92	16.1	10.05	-3.91
V	94	30.7	14.70	1.45
VI	91	25.4	15.37	0.10
VI	92	37.1	23.80	-6.11

TABLE 3

POLYNOMIAL FITS

Polynomial	Average Error
I. $f(\theta) = a + b\theta + c\theta^2$	1.090 db
II. $f(\theta) = a + b\theta^{-1} + c\theta^2$	0.314 db
III. $f(\theta) = a + b\ln\theta + ce^{\theta}$	0.673 db
IV. $f(\theta) = a + b\theta^{0.4} + c\theta^{0.9}$	0.525 db

TABLE 4

PARAMETER AVERAGES

$$\sigma^0 = A + B\theta^{-1} + C\theta^2$$

Type	Line	A	B
I	91	-4.73	6.2
II	91	-5.30	15.0
II	94	-12.01	48.8
III	91	-3.49	-11.1
IV	91	-8.64	89.5
V	92	-3.74	12.2
V	94	-9.15	2.4
VI	91	-6.60	29.3
VI	92	-17.00	55.1

TABLE 5

PATTERN CLASSIFICATION RESULTS

	No. Pts.	Correct	Related Type	Incorrect
Line 91				
Type I (F)	11	8	3	0
Type II (F)	5	4	1	0
Type III (F)	5	3	2	0
Type IV (W)	20	18	0	2
Type VI (F)	8	7	1	0
Line 92				
Type V (M)	40	40	0	0
Type VI (F)	10	10	0	0
Line 94				
Type II (F)	12	12	0	0
Type V (M)	17	17	0	0

W - Water
F - First-Year
M - Multi-Year

TABLE 6

AVERAGE VALUES

SLOPE-AVERAGE

Type	Line	Slope	Average
I	91	-.166	-7.77
II	91	-.275	-8.07
II	94	-.397	-13.60
III	91	-.186	-7.73
IV	91	-.550	-8.83
V	92	-.183	-9.74
V	94	-.273	-6.96
VI	91	-.244	-7.79
VI	92	-.254	-15.70
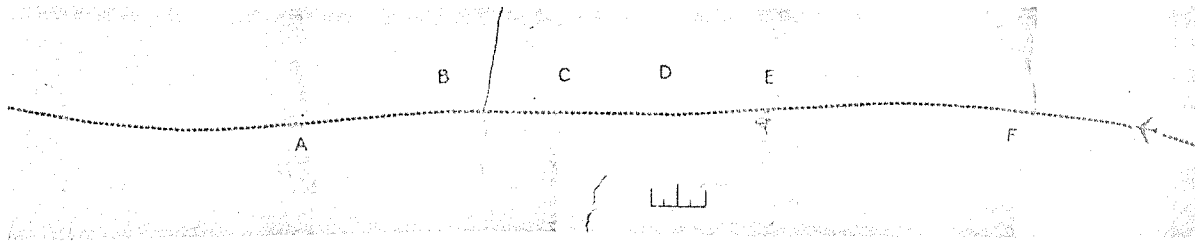
Air Photo Mosaic: Arctic Pack Ice, Beaufort Sea, 15 May 1967, line 92
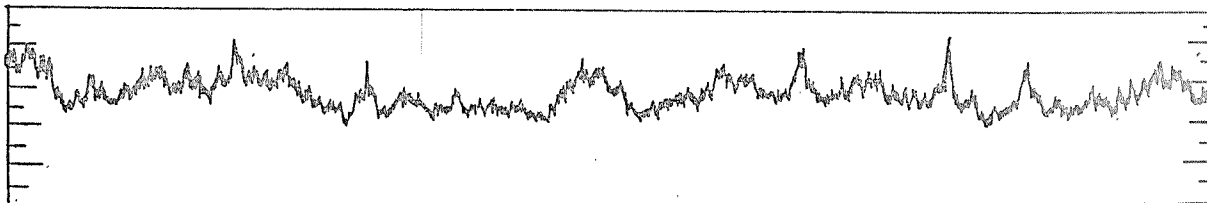
Radar Return at 7.2° Incidence Angle
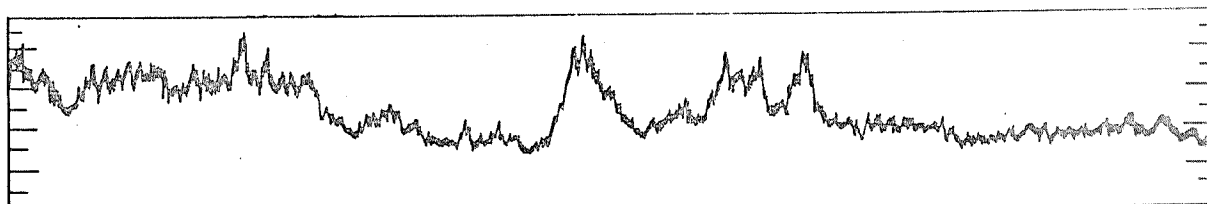
Radar Return at 25° Incidence Angle
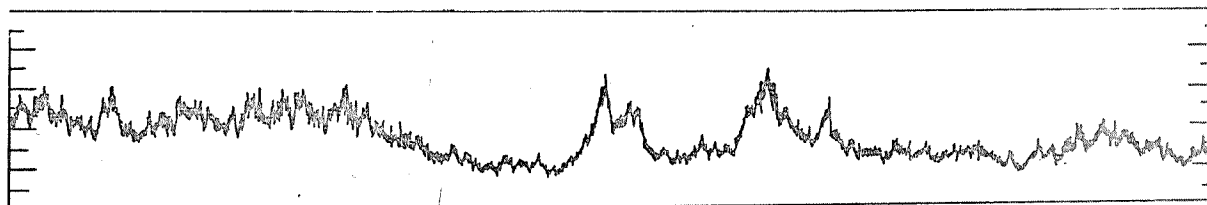
Radar Return at 45° Incidence Angle
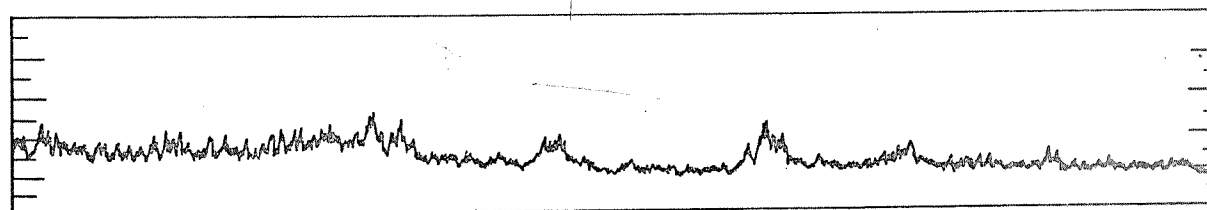
Radar Return at 51.5° Incidence Angle
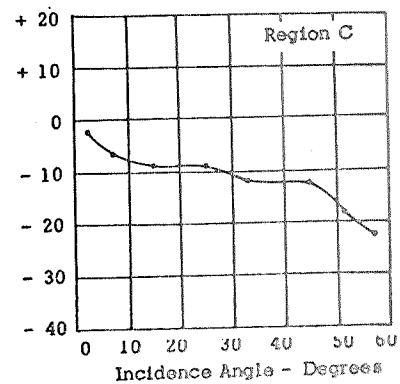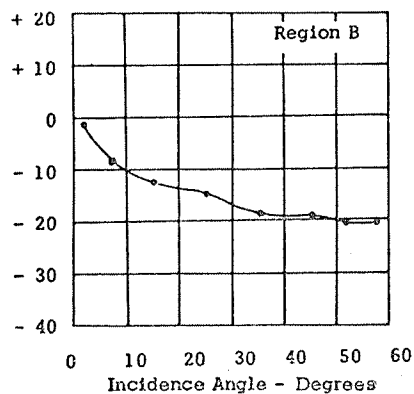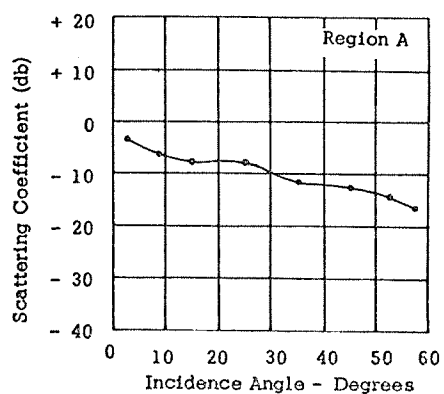
FIGURE 1   LINE 92
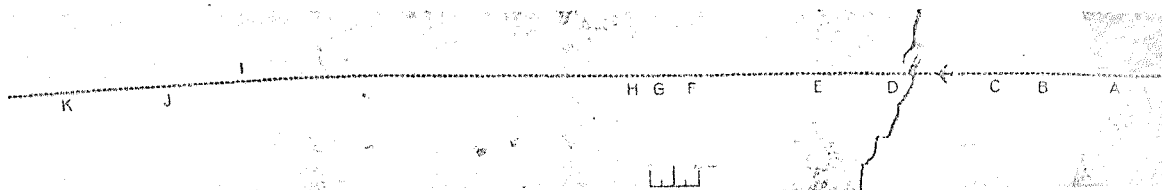
Air Photo Mosaic: Arctic Pack Ice, Beaufort Sea, 15 May 1967, line 94
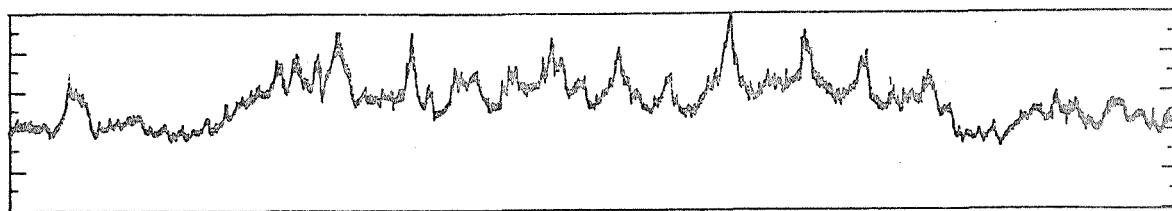
Radar Return at 7.2° Incidence Angle
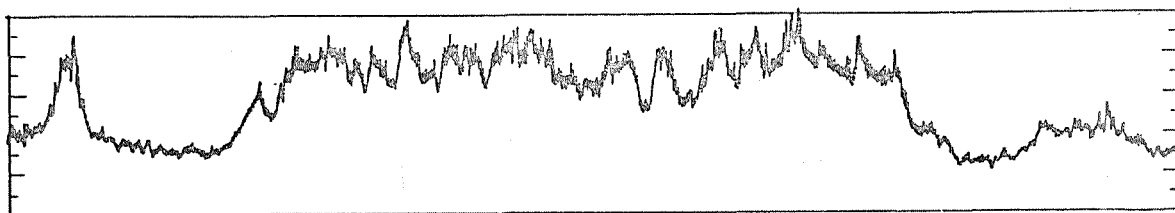
Radar Return at 25° Incidence Angle
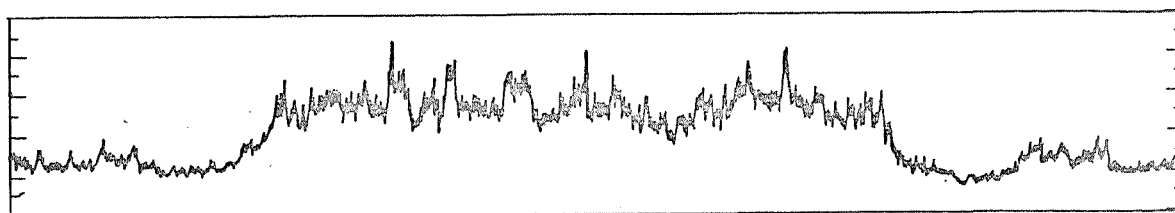
Radar Return at 45° Incidence Angle
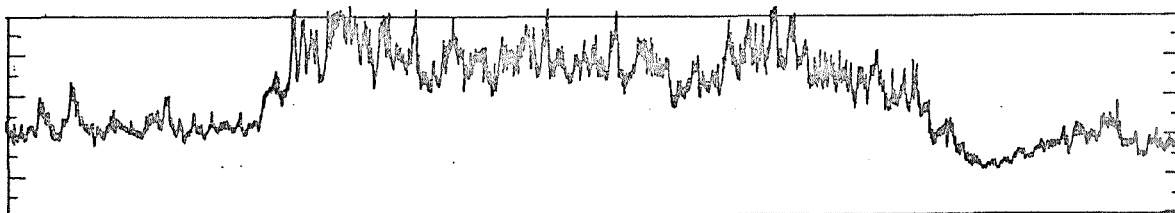
Radar Return at 51.5° Incidence Angle
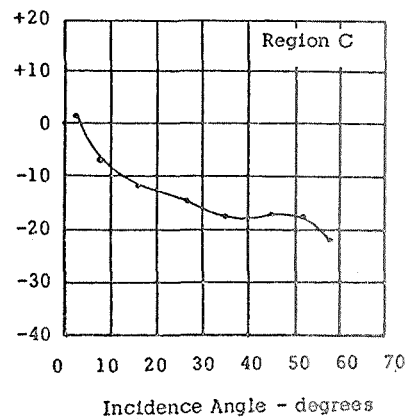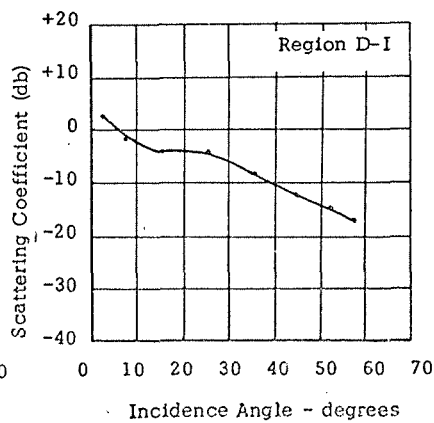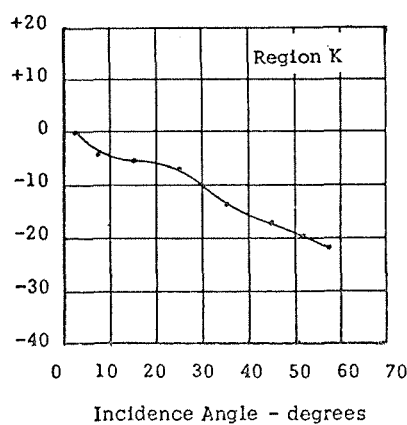
FIGURE 2   LINE 94

Figure 3 Line 94

Comparison of Scatterometer Data
7.2° and 51.7° incidence angles

Scattering coefficient (db) 7.2° incidence angle

Scattering coefficient (db) 51.7° incidence angle
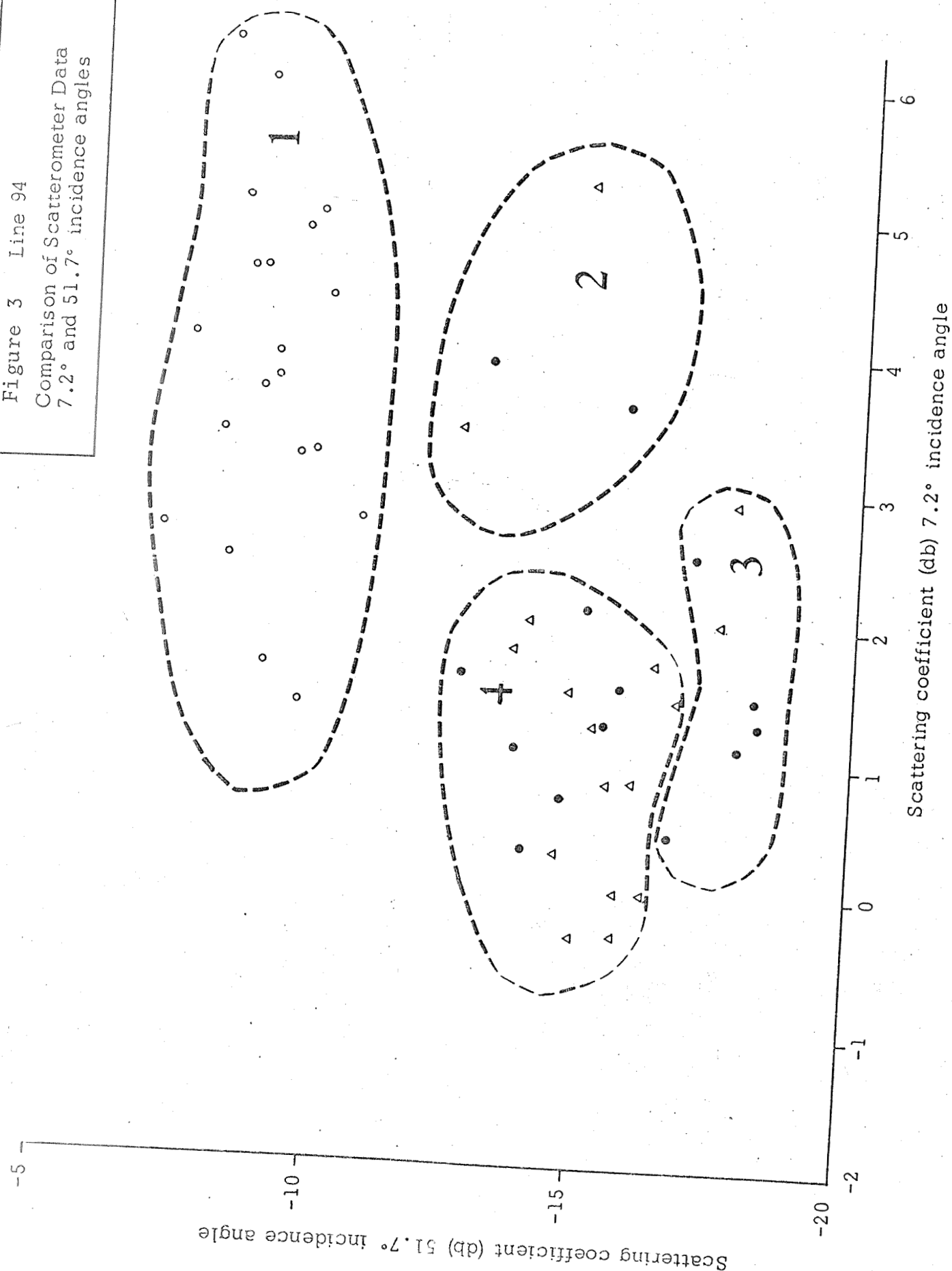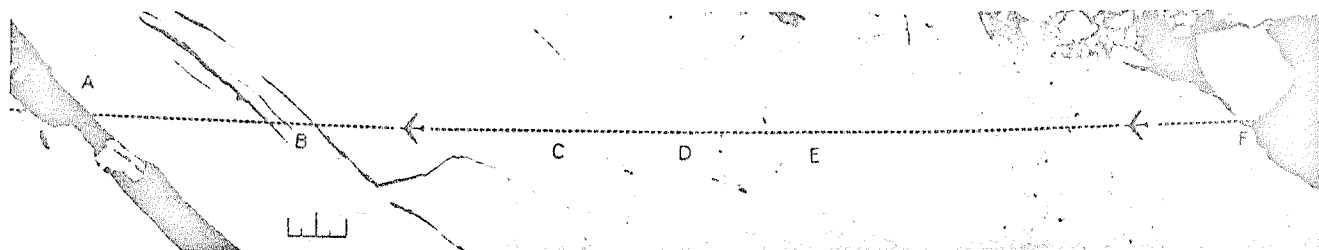
Air Photo Mosaic: Arctic Ice, Off Shore of Barrow, Alaska, 12 May 1967, line 91
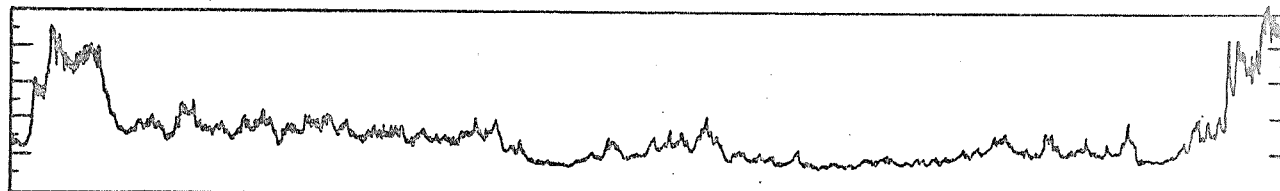
Radar Return at 2.5° Incidence Angle
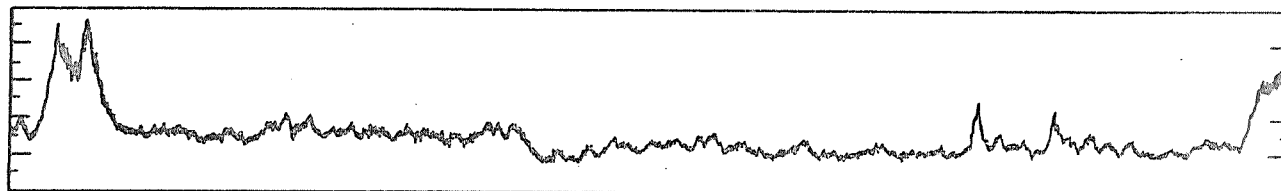
Radar Return at 6.7° Incidence Angle
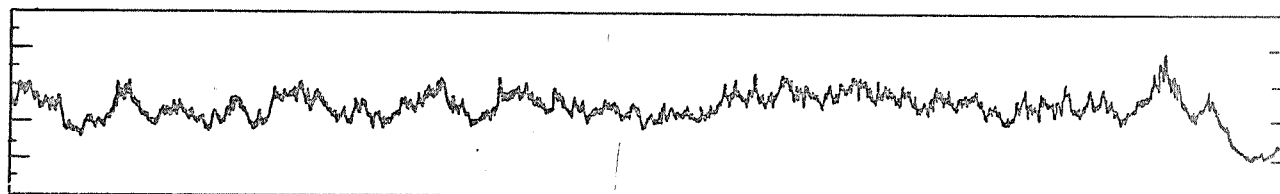
Radar Return at 25.0° Incidence Angle
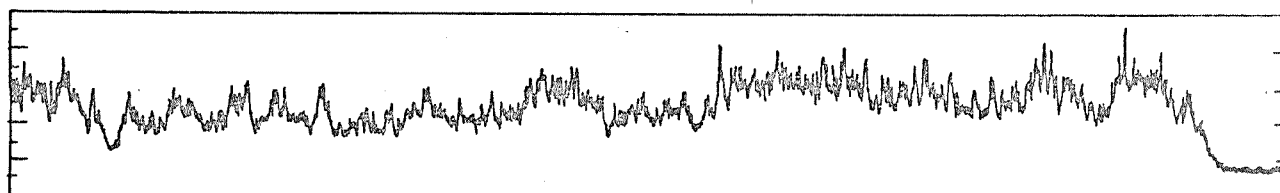
Radar Return at 52.1° Incidence Angle
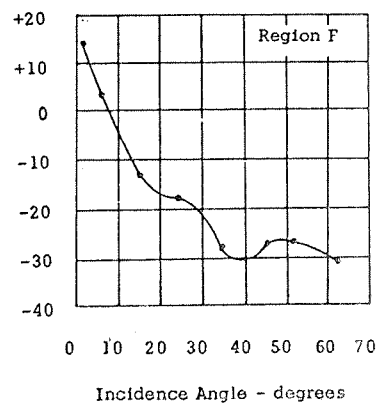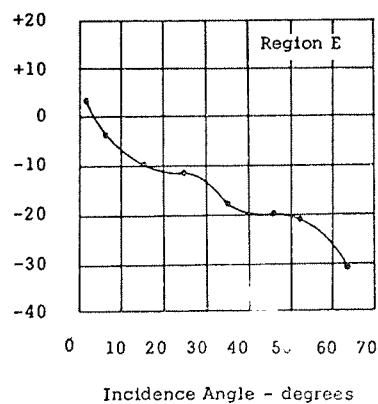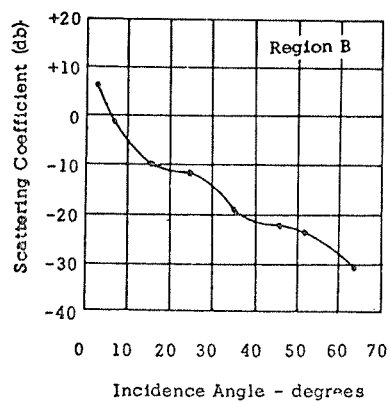
FIGURE 4   LINE 91
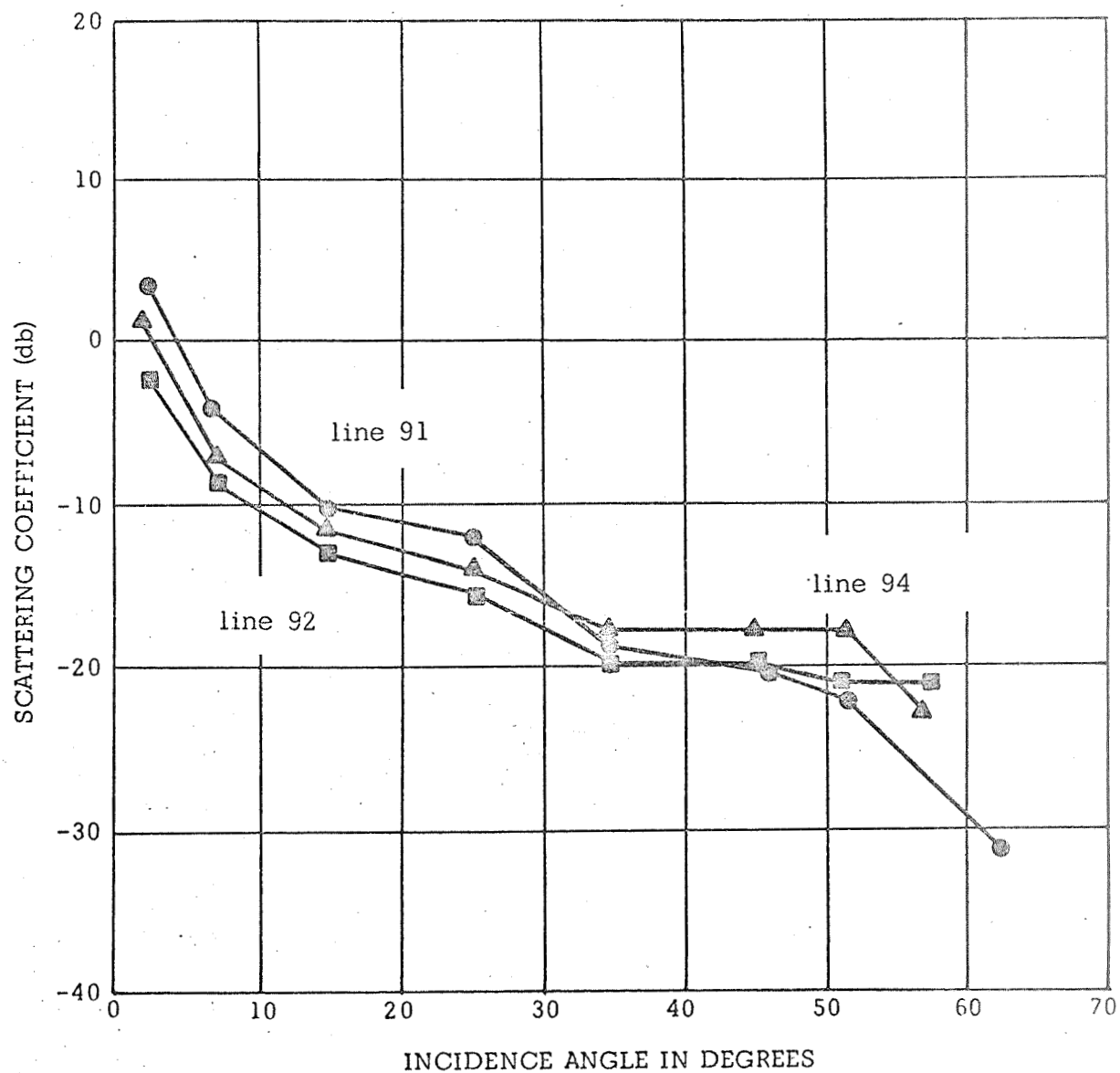
Figure 5 Scattering coefficient variations for first-year ice
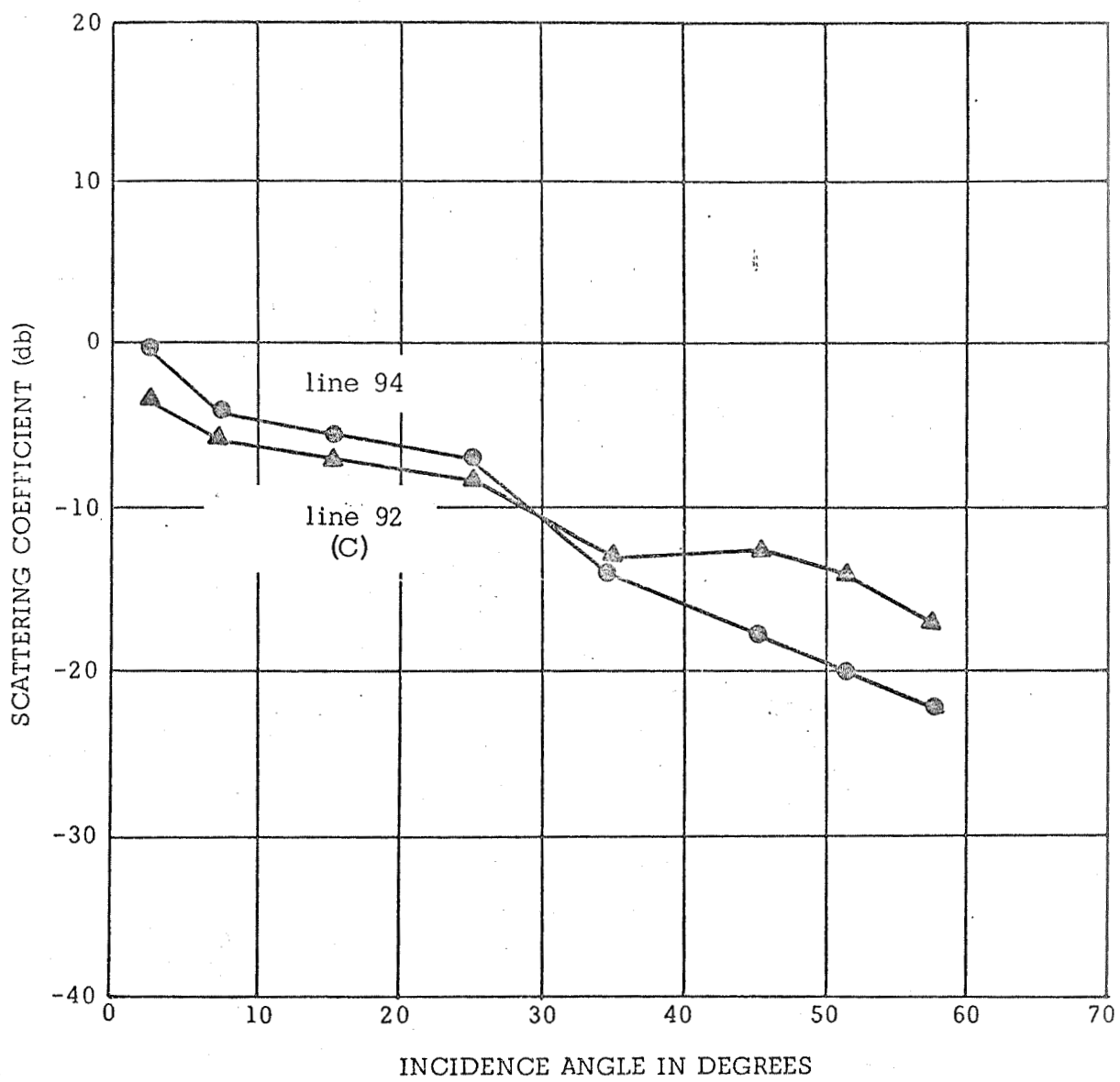
Figure 6   Comparison of scattering coefficient variations for multi-year ice

FIGURE 7

CLASSIFIED CLUSTER PLOT

MODIFIED KIRCHHOFF EQUATION

LINE 91
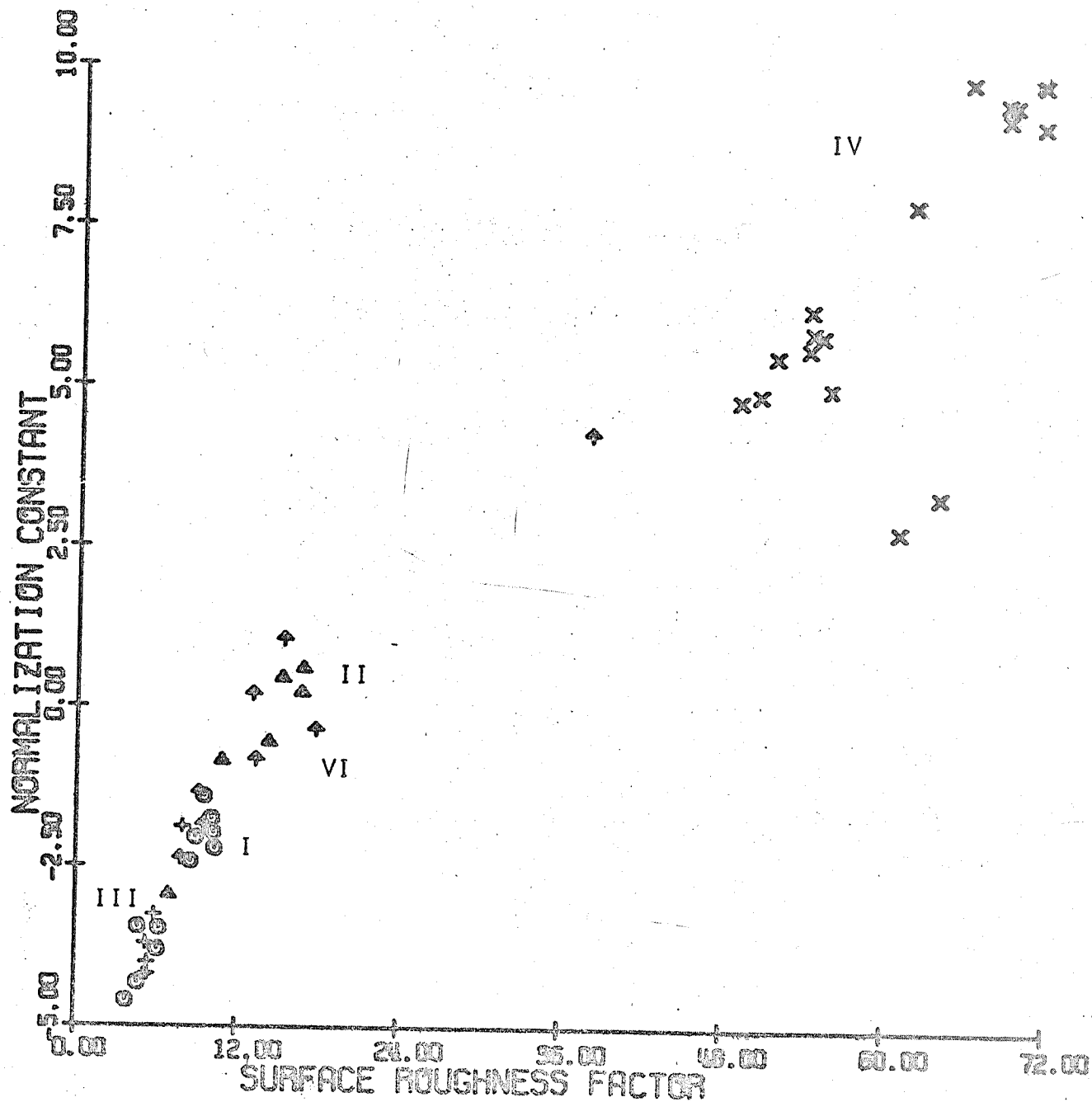
FIGURE 8

CLASSIFIED CLUSTER PLOT

MODIFIED KIRCHHOFF EQUATION

LINE 92
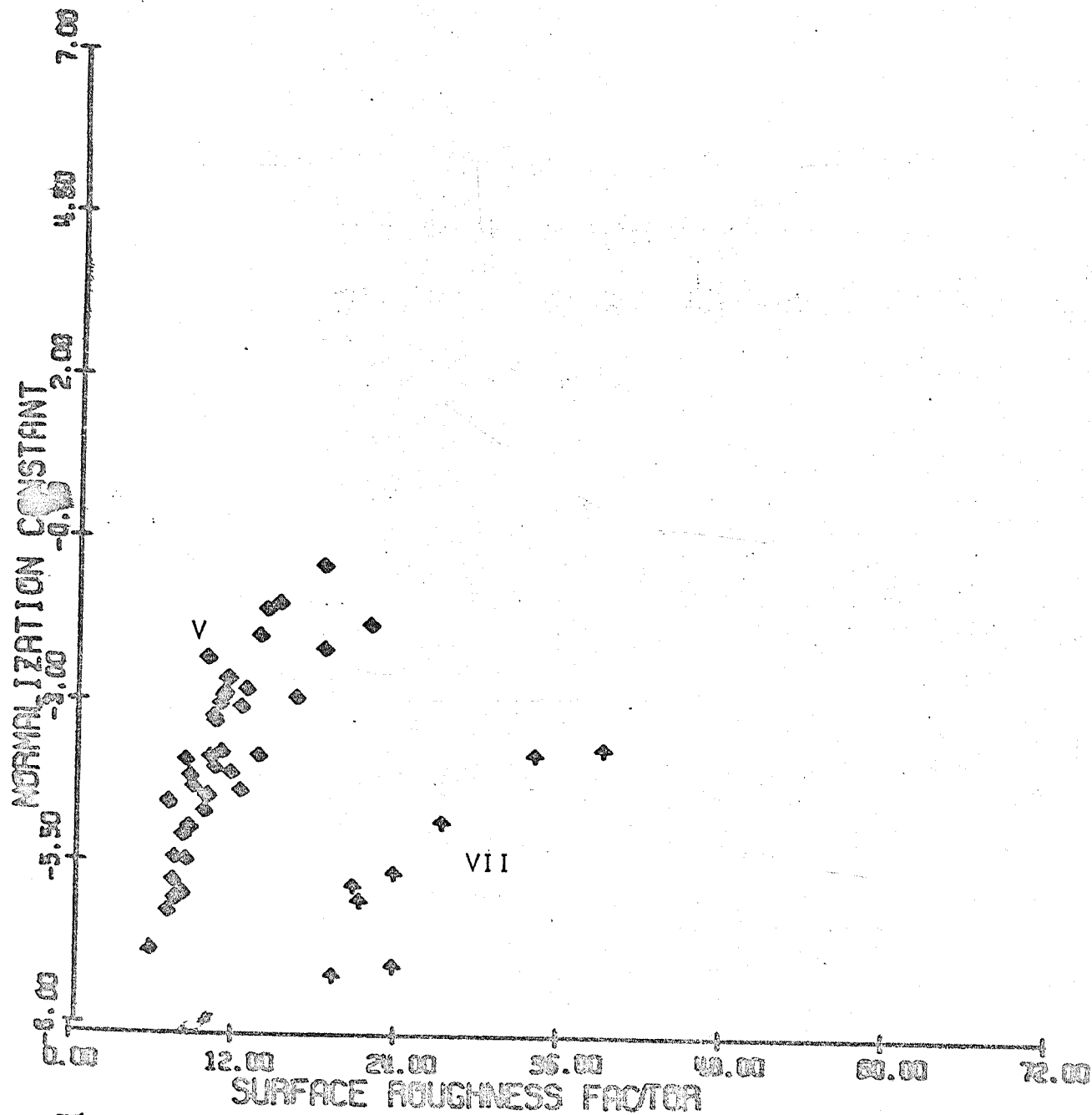
FIGURE 9

CLASSIFIED CLUSTER PLOT

MODIFIED KIRCHHOFF EQUATION

LINE 94
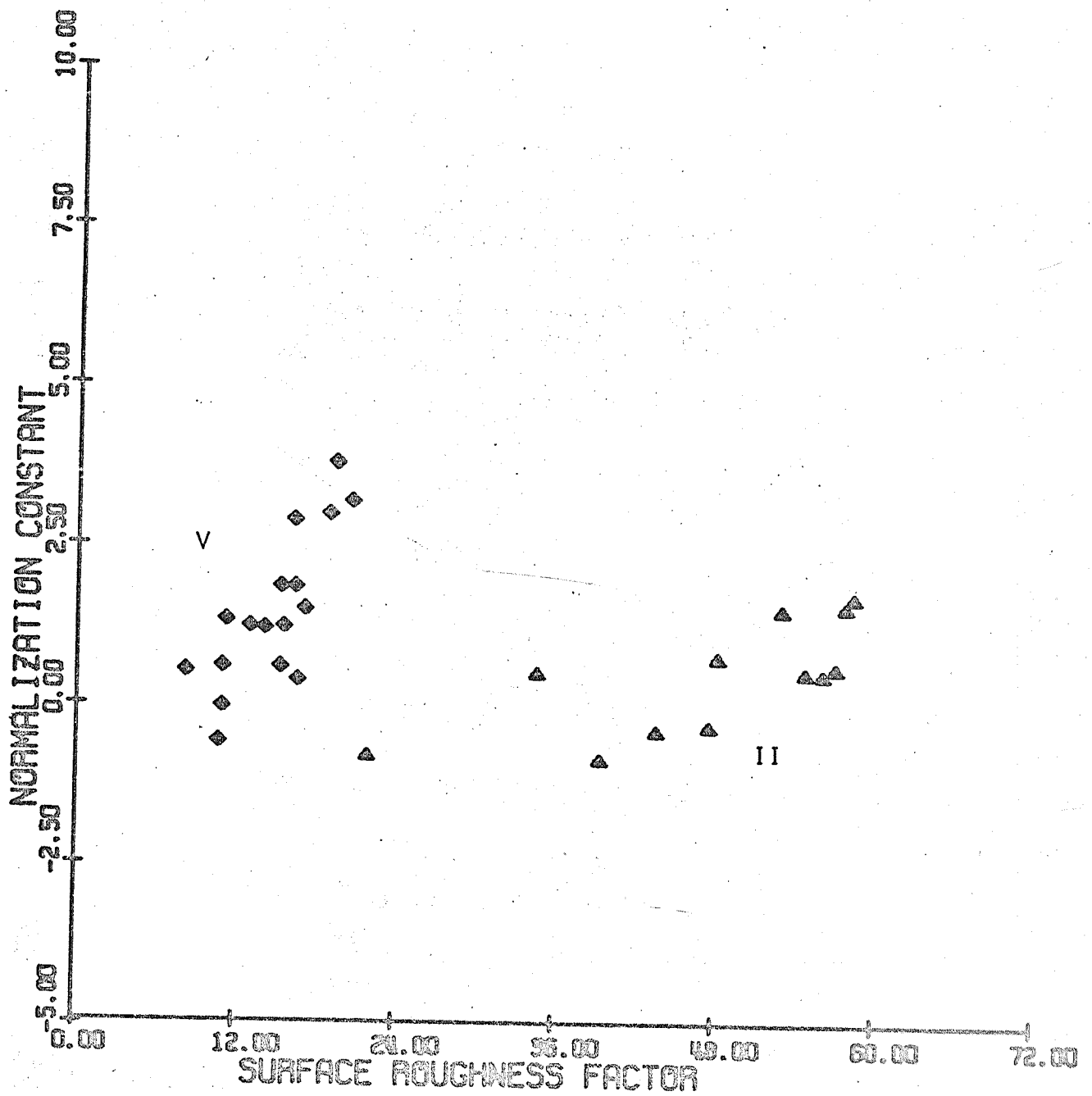
FIGURE 10

CLASSIFIED CLUSTER PLOT

POLYNOMIAL PARAMETERS

LINE 91
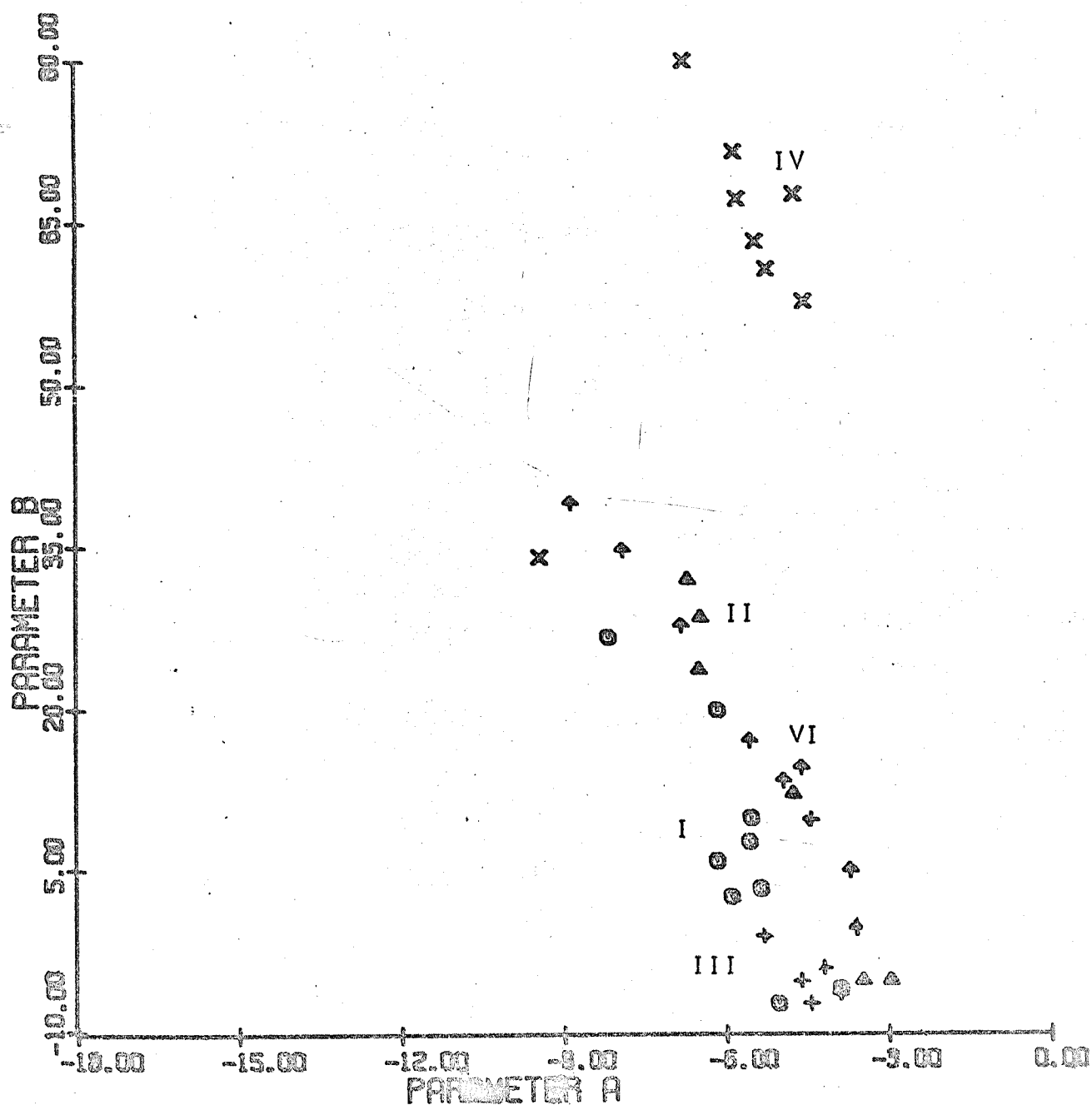
FIGURE 11

CLASSIFIED CLUSTER PLOT

POLYNOMIAL PARAMETERS

LINE 92
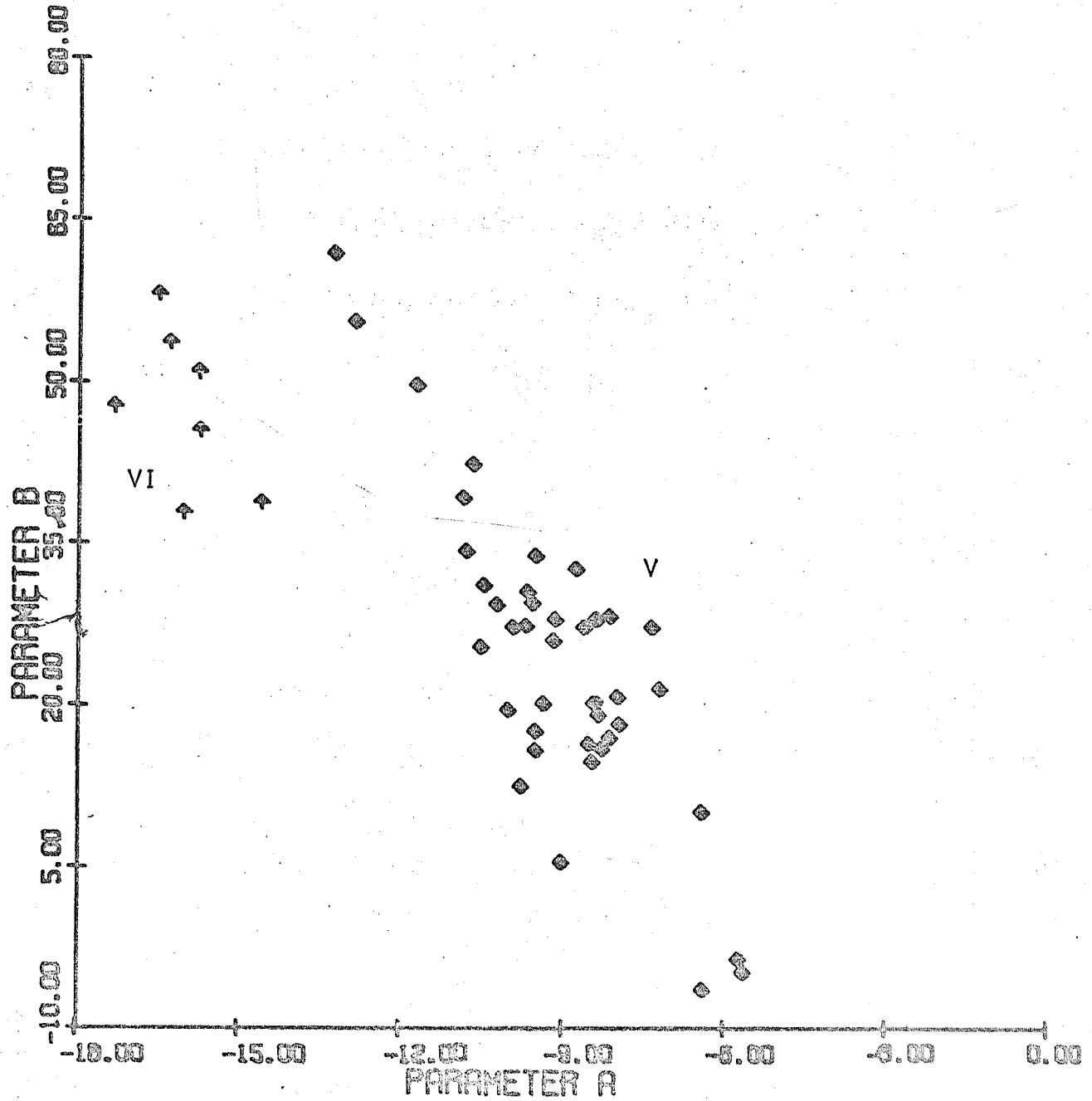
FIGURE 12

CLASSIFIED CLUSTER PLOT

POLYNOMIAL PARAMETERS

LINE 31
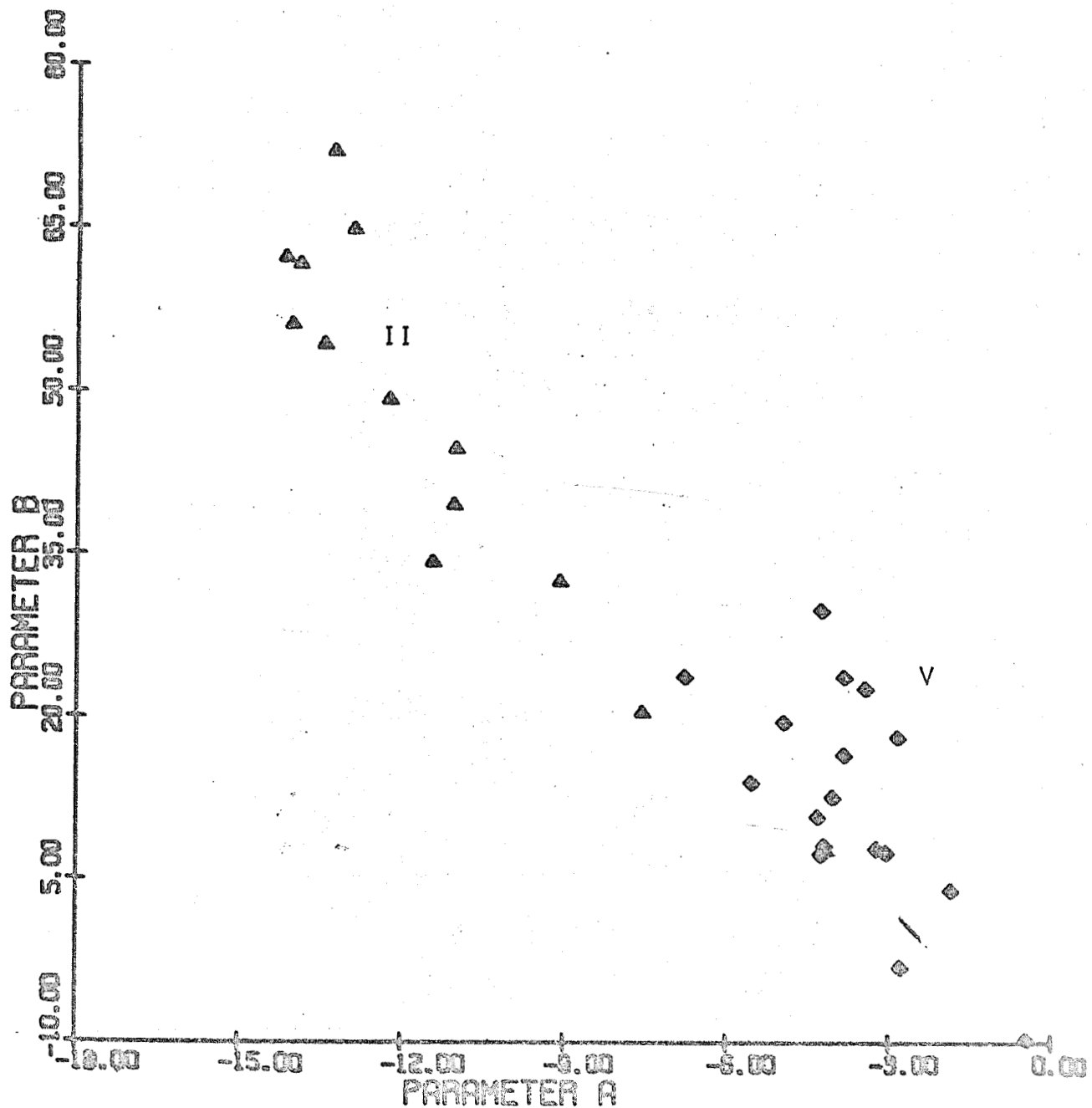
FIGURE 13

CLASSIFIED CLUSTER PLOT

SLOPE—AVERAGE VALUE
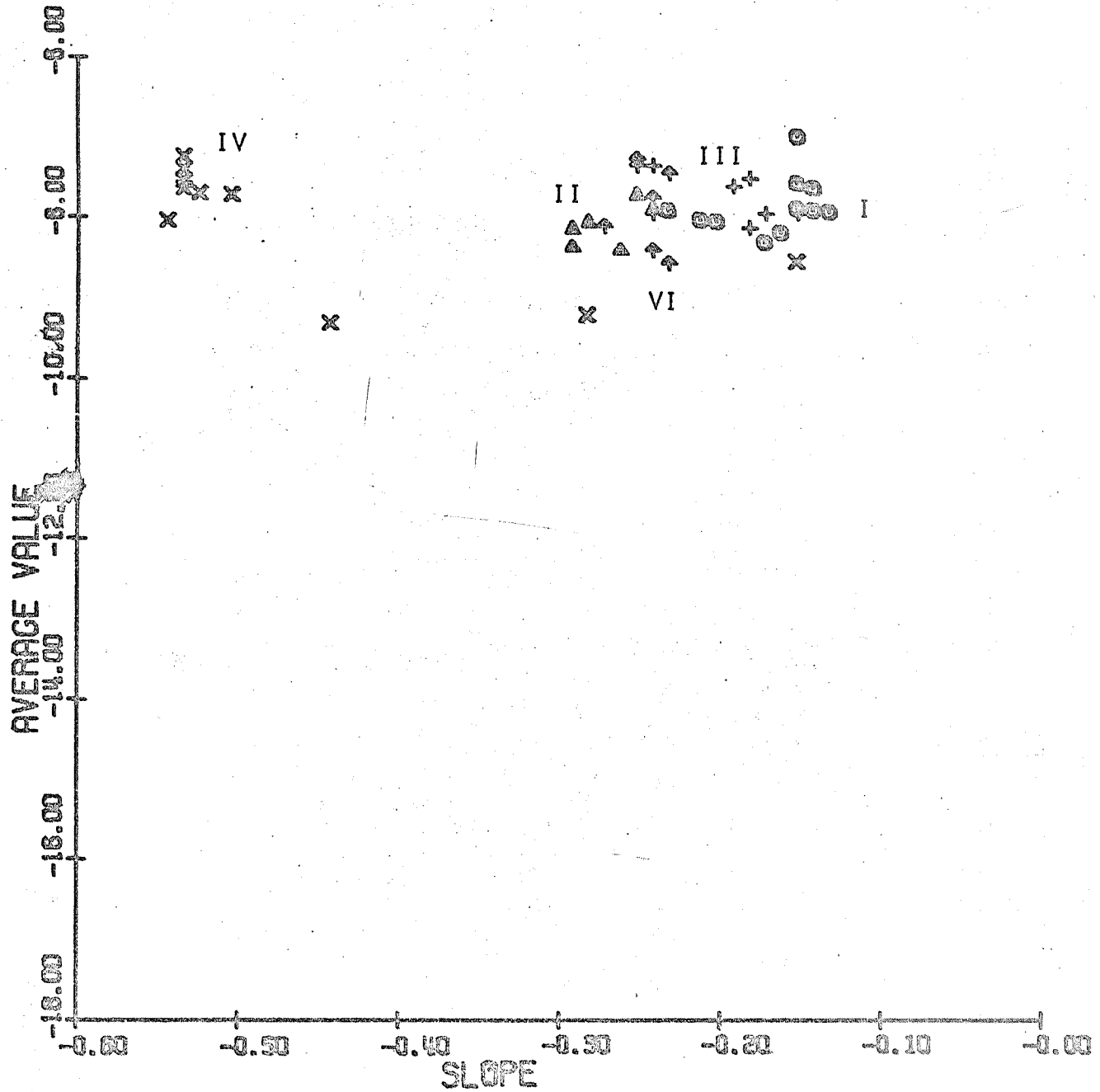
LINE 91

FIGURE 14

CLASSIFIED CLUSTER PLOT

SLOPE—AVERAGE VALUE

LINE 92
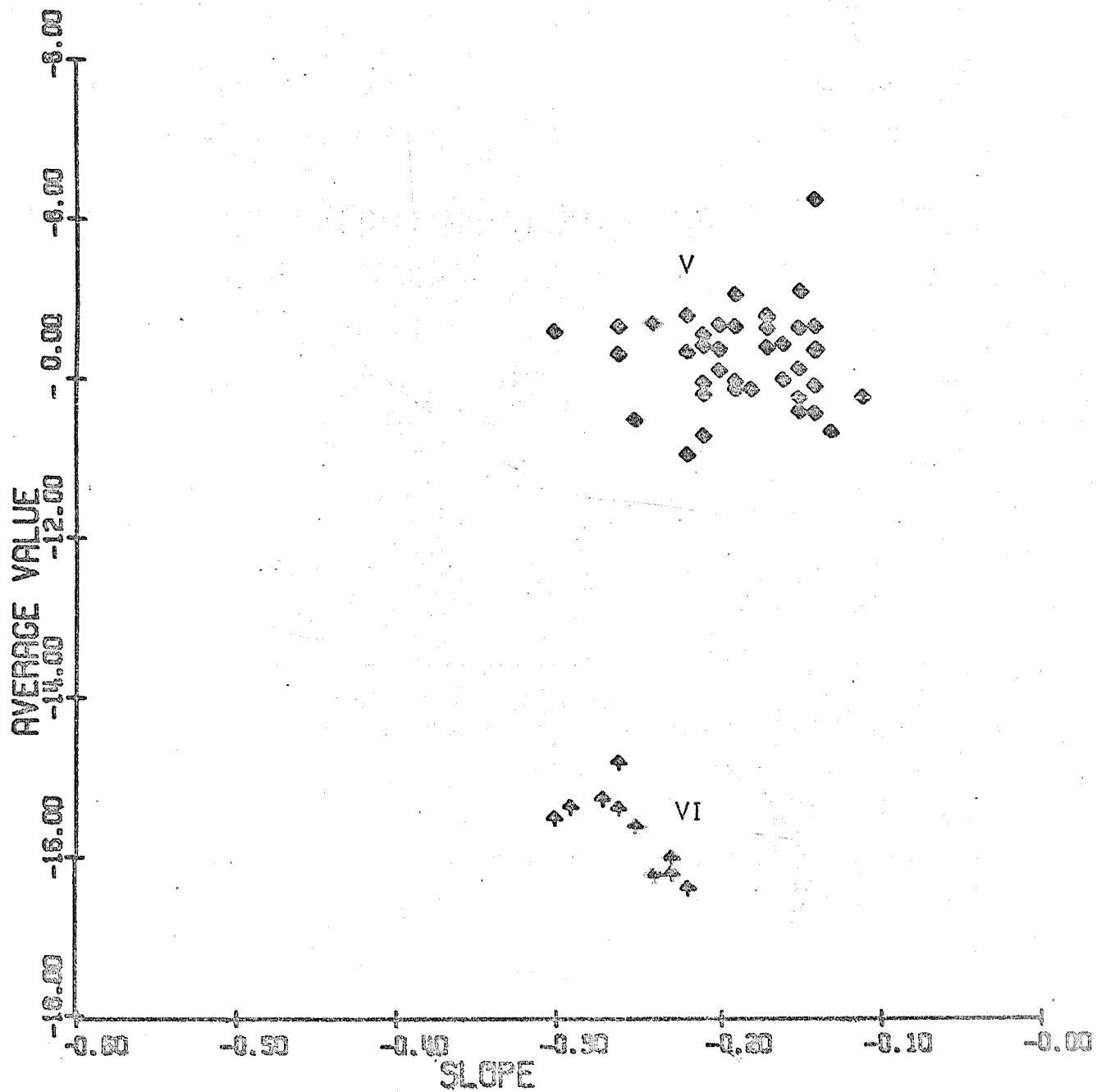
FIGURE 15

CLASSIFIED CLUSTER PLOT

SLOPE--AVERAGE VALUE

LINE 94
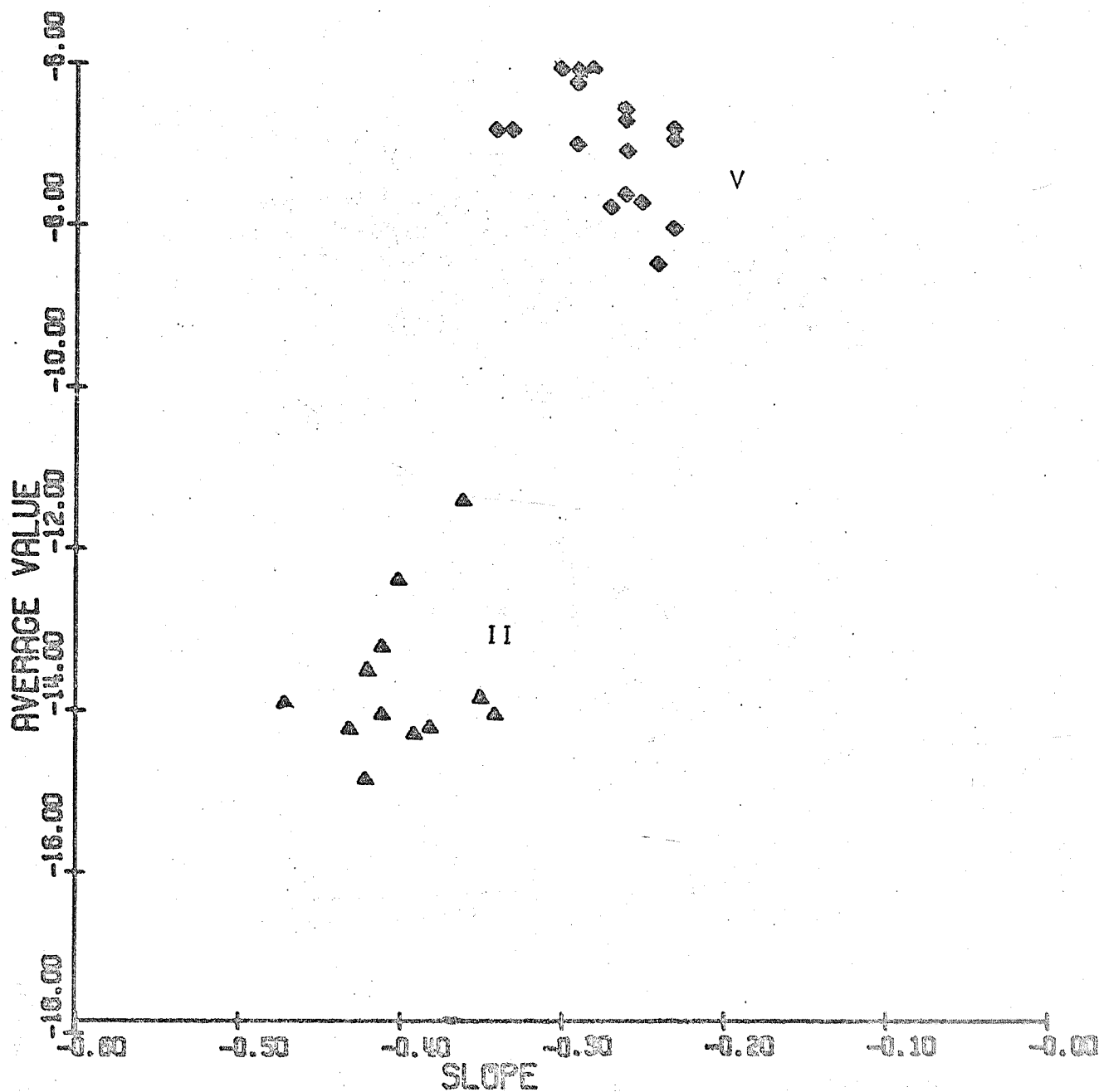
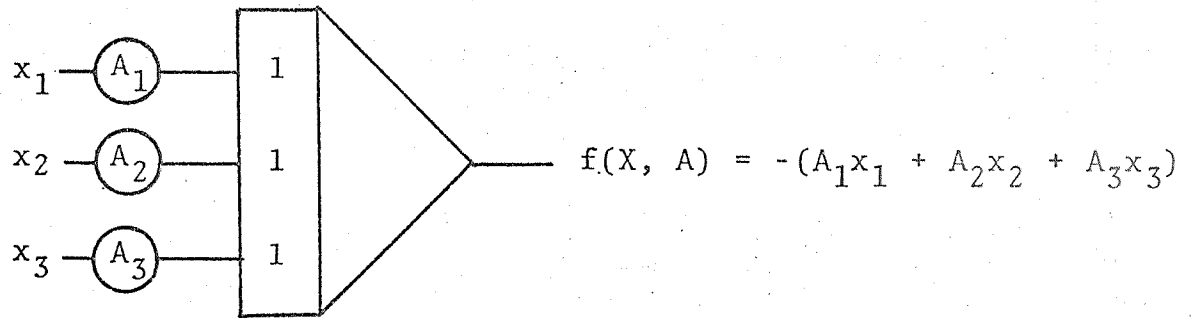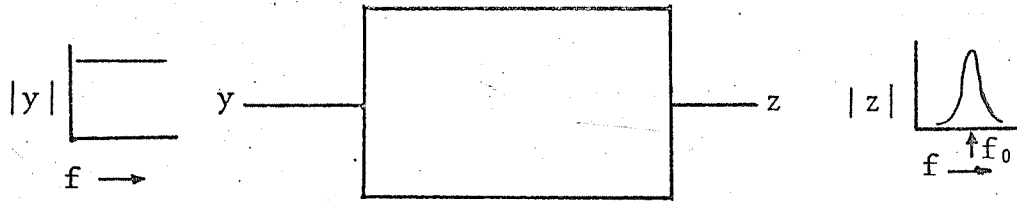FIGURE 16

CLUSTER PLOT

SLOPE--AVERAGE VALUE

LINE 91,92,94
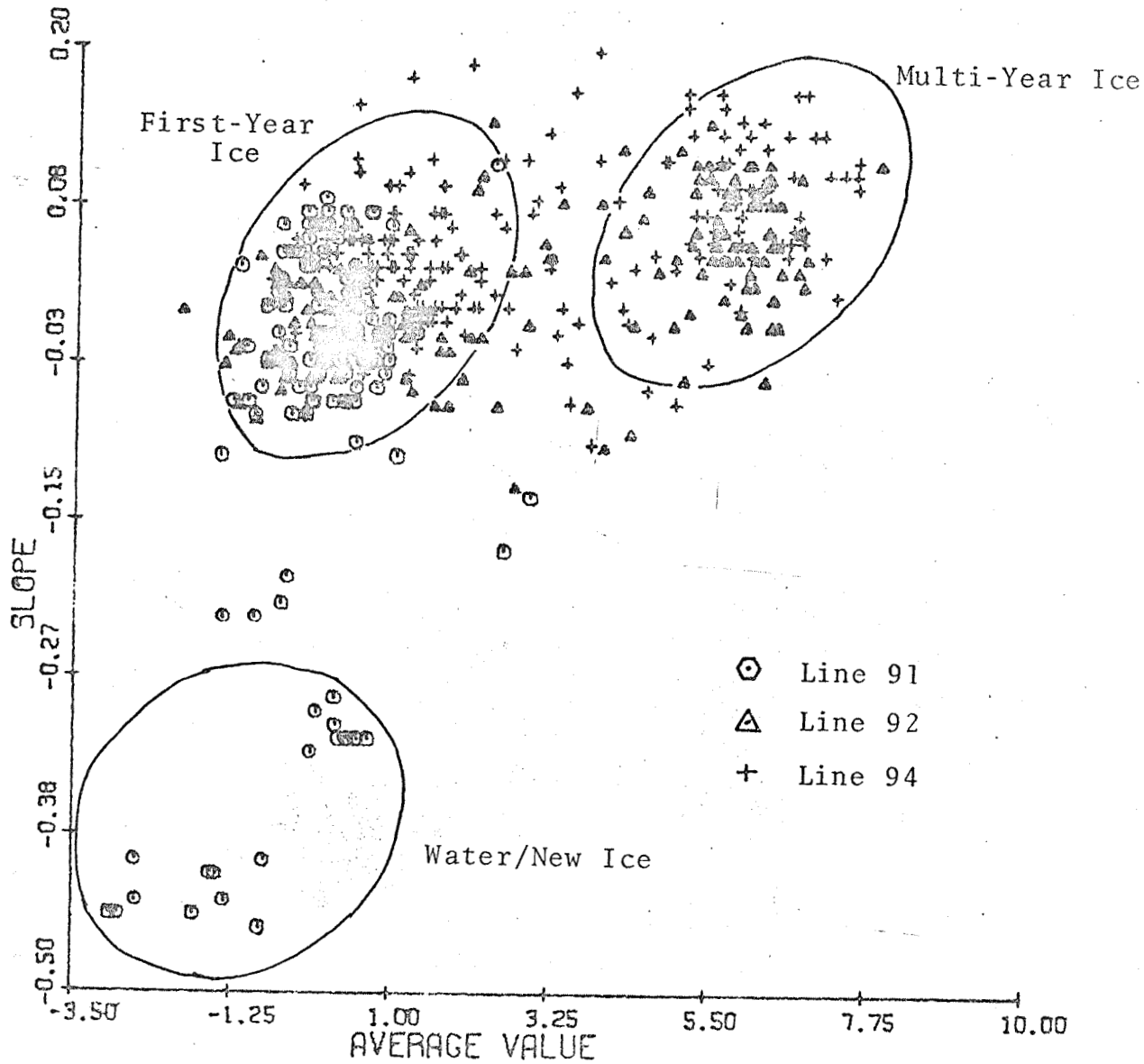
FIGURE 17

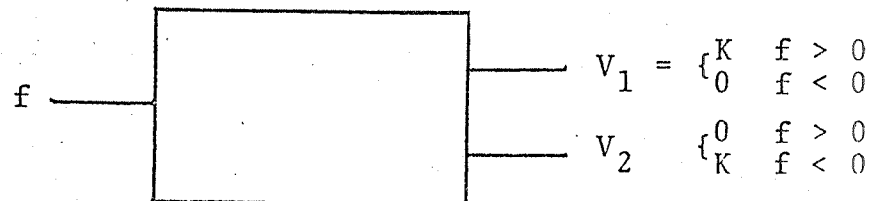ANALOG CIRCUITS

$$f(X, A) = -(A_1 x_1 + A_2 x_2 + A_3 x_3)$$

ADDER

BAND PASS FILTER

$$V_1 = \begin{cases} K & f > 0 \\ 0 & f < 0 \end{cases}$$

$$V_2 \quad \begin{cases} 0 & f > 0 \\ K & f < 0 \end{cases}$$
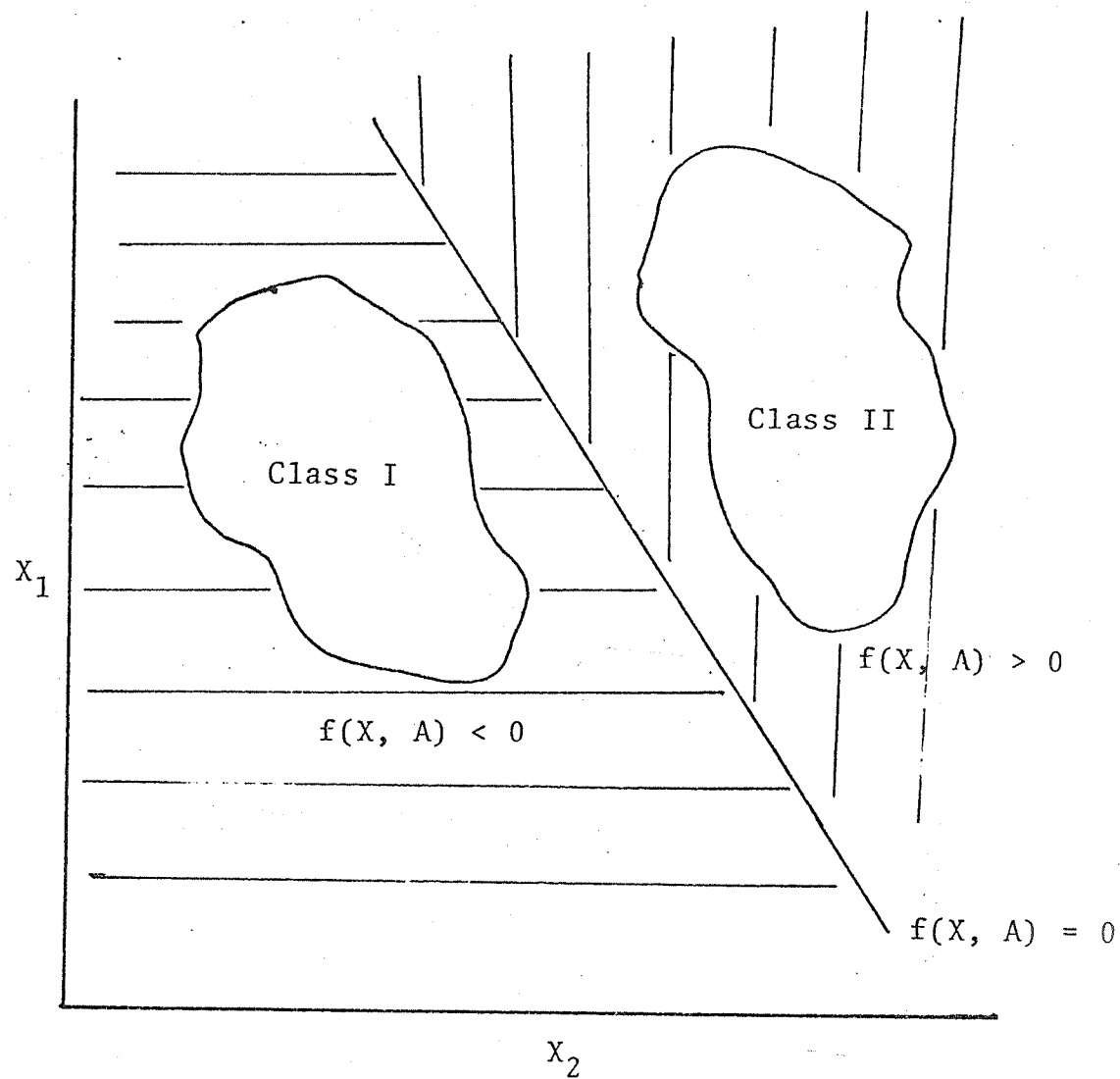
COMPARATOR

FIGURE 18

CLASSIFICATION ANALYSIS

FIGURE 19

ANALOG SIMULATION OF SCATTEROMETER CLASSIFICATION SYSTEM